Fuel 381 (2025) 133561

Contents lists available at ScienceDirect

Fuel

journal homepage: www.elsevier.com/locate/fuel

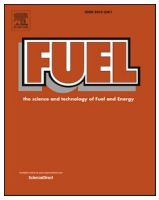

Full Length Article

Operation of a differential fixed bed reactor for investigations on micro-kinetics of heterogeneous gasification reactions

Stella Walker [a,b,*], Thomas Kolb [a,b]

[a] Karlsruhe Institute of Technology, Engler-Bunte-Institute, Fuel Technology, EBI-ceb, Engler-Bunte-Ring 1, 76131 Karlsruhe, Germany
[b] Karlsruhe Institute of Technology, Institute for Technical Chemistry, ITC-vgt, Hermann-von-Helmholtz-Platz 1, 76344 Eggenstein-Leopoldshafen, Germany

ARTICLE INFO

Keywords:
Pressurized gasification kinetics
System response behavior
Differential fixed bed reactor
Heterogeneous reaction kinetics
Char conversion

ABSTRACT

A pressurized differential fixed bed reactor (dFBR) developed for the investigation of micro-kinetics of heterogeneous reactions is presented in this work. The operability of the dFBR is assessed by the example of gasification experiments with biogenic char and steam. Two main challenges are addressed: the definition and verification of differential operation and the influence of the system response behavior on the derived reaction kinetics. Based on the first Damköhler number, a threshold value of the ratio between the reaction gas concentration $c_{i,H}$ leaving the differential fixed bed and the concentration $c_{i,0}$ entering was derived as a new criterion for differential operation. For a ratio of $c_{i,H}/c_{i,0} \geq 0.9$, the fixed bed reactor is operated differentially. To determine the influence of the system response behavior on the reaction kinetics, system responses were investigated for a set of different reactor temperatures, total pressures and reaction gas compositions. Then, the system-specific response behavior was described based on the axial dispersion model. The description was integrated into the experimental data evaluation routine. Subsequently, the influence of the system response behavior on the derived kinetics was assessed by means of the ratio between the reciprocal value of the reactivity $1/R_{UCM-C}$ to the spread of the residence time distribution E(t). It was found that for ratios of six or lower, the system response behavior relevantly affected the experimental results.

1. Introduction

This paper deals with the development and operation of a differential reactor for investigation on micro-kinetics of heterogeneous reactions at elevated pressures. The operation is demonstrated for the heterogeneous water–gas reaction (r1) and the Boudouard reaction (r2) of beech wood char particles.

$$r1: C + H_2O \rightarrow CO + H_2 \quad (1)$$

$$r2: C + CO_2 \rightarrow 2\,CO \quad (2)$$

The investigation of these micro-kinetics is part of the research on a process chain consisting of pyrolysis, entrained flow gasification and subsequent synthesis for biogenic and anthropogenic waste material investigated at Karlsruhe Institute of Technology (KIT) [1]. Fundamental research on the conversion of solid, carbon-rich particles by heterogeneous gasification requires an experimental setup allowing for different reaction gas atmospheres at elevated pressure as well as uniform, well-defined reaction conditions for the fuel sample.

This comprises that concentration gradients in the reactive zone (e.g. sample bed) have to be avoided. Furthermore, at high reaction temperatures, the measured effective reaction rates are dominated by the mass transport rates being slow compared to the micro-kinetics. Low reaction temperatures ensure that the mass transport from the gas phase to the outer particle surface (film diffusion) and through the porous structure of the particle to the inner surface (particle diffusion) is faster than the micro-kinetics [2]. This corresponds to the chemical regime by Rossberg and Wicke [3], which belongs to temperatures below 900 °C for the heterogeneous gasification reactions of wood char particles with particle sizes up to 150 µm [2,4].

Different types of lab-scale reactors have been established to meet these demands, the most common ones being the thermogravimetric analyzer (TGA), fixed bed reactors, drop-tube reactors (DTR), fluidized bed reactors (FBR) and wire mesh reactors (WMR) [2].

The choice of the reactor type depends on various factors, mainly reaction temperature and reaction gas partial pressure. Most commonly, gasification kinetics are determined with TGAs (62 %). To a lesser extent, gasification experiments are carried out in fixed or packed bed

* Corresponding author.
E-mail address: stella.walker@kit.edu (S. Walker).

https://doi.org/10.1016/j.fuel.2024.133561
Received 2 August 2024; Received in revised form 19 October 2024; Accepted 25 October 2024
Available online 1 November 2024
0016-2361/© 2024 The Authors. Published by Elsevier Ltd. This is an open access article under the CC BY-NC-ND license (http://creativecommons.org/licenses/by-nc-nd/4.0/).

Nomenclature

Glossary

Symbol	Description Unit (SI)
Bo	Bodenstein number (−)
c	concentration (mol/m^3)
D_{ax}	axial dispersion coefficient (m^2/s)
d	diameter (mm)
d_a	outer diameter of quartz glass sample holder (mm)
Da_I	first Damköhler number (−)
d_h	hydraulic diameter (m)
D_m	molecular diffusion coefficient (m^2/s)
E	residence time distribution (−)
erfc	complementary error function (Gauß)
ε_A	change in volume flow ε_A for the plug flow reactor (−)
f_1, f_2	fitting parameters of the axial dispersion model ($s^{0.5}$, $s^{-0.5}$)
F	transfer function (primitive of E) (−)
Fo	Fourier number for mass transport (−)
H	height of a fixed bed (m)
k	rate constant for kinetics (variable)
L	length of a flow channel / pipe / the reactor (m)
$\widetilde{M}$	molar mass (g/mol)
m_0	char sample mass weighed for an experiment (g)
m	mass (g)
$\dot{n}$	molar flow rate (mol/s)
n	reaction order (−)
p	pressure / partial pressure (bar)
Pe_{ax}	axial Péclet number (−)
ϕ	Thiele modulus (−)
R	reactivity (1/s)
r	reaction rate (mol/g/s)
$r_{channel}$	radius of a channel (m)
Re	Reynolds number (−)
ρ	density (kg/m^3)
Sc	Schmidt number (−)
s_w	wall thickness of quartz glass sample holder (mm)
T	temperature (K or °C)
t	time (s)
τ	residence time (hydrodynamic) (s)
t_D	time constant for diffusion (s)
τ_{mod}	modified residence time for Da_I (kg/s/m^3)
t_R	reaction time scale (s)
t_τ	transport time scale (s)
u_{gas}	gas flow velocity (m/s)
$\dot{V}$	volume flow (m^3/s)
X	conversion (−)
x or z	axial coordinate (m)
y	molar fraction (−)

Subscript	Description
bed	fixed bed
C	carbon
calc	calculated
conv	converted
eff	effective
exp	experiment
gasif	gasified (total amount of gasified carbon)
H_2O	H_2O gasification atmosphere
i	refers to variable species (CO_2 or H_2O) or time step
in	entering the system
m	refers to mass
mix	mixed gasification atmosphere (CO_2 + H_2O)
mod	modified for definition of Da_I
obs	observed
out	leaving the system
part	particles in the sample bed
Prod	product gases
reactor	reactor tube of the dFBR
tot	total
UCM	Uniform Conversion Model
UCM-C	processing the reaction kinetic data to the convoluted UCM model
V	refers to volume

Abbreviation	Description
µGC	micro gas chromatograph
CEM	controlled evaporation and mixing
CSTR	continuously stirred tank reactor
dFBR	differential fixed bed reactor
DTR	drop-tube reactor
EFG	entrained flow gasification
FBR	fluidized bed reactor
MFC	mass-flow controller
STP	standard temperature and pressure (273 K, 1.013 bar)
TGA	thermogravimetric analyzer
UCM-C	processing the reaction kinetic data to the convoluted UCM model
WMR	Wire mesh reactor

reactors (18.5 %), DTRs (7.6 %) and FBRs (5.4 %) [2]. The basis of the evaluation of experimental data is to determine the time-dependent conversion X_C of fixed carbon in the sample m_C (equation (3)).

$$X_C(t) = \frac{m_C(t=0) - m_C(t)}{m_C(t=0)} \tag{3}$$

In the TGA, the sample mass in a crucible is measured over time during reaction. The gas transport in the crucible and the sample bed is mainly dominated by diffusion and influenced by temperature, pressure, crucible geometry and sample bed height [2,4,5]. Kibria et al. [4] investigated the influence of different factors such as sample weight, particle structure, crucible geometries and CO_2 flow rate on the conversion rate of pine bark char at 700 °C to 1100 °C. They demonstrated that diffusion effects through the sample bed can be minimized by applying low sample masses that form a monolayer of particles in the crucible, sufficiently high gas flow rates and flat crucibles. The particle structure (particle size and pore morphology) can influence the conversion rate in both directions. A systematic approach is given to optimize the considered parameters for specific samples [4].

Baath et al. [5] studied the influence of diffusion and heat transfer processes on the gasification reaction and particle conversion in CO_2 in TGA experiments by modelling the char particle conversion and heat and mass transport processes. The modelling results were compared to gasification experiments with biochar particles of 200 µm at 800 °C to 900 °C in CO_2. Comparably high sample masses of 25 mg were applied in a crucible with a diameter of 5.5 mm. Their calculations showed that at gasification temperatures of 900 °C, the activation energy apparently decreases by 8.5 % when determined without considering heat and mass transport, with the greatest impact being assigned to the mass transport through the sample bed [5].

Stoesser et al. [2] conducted CO_2 gasification experiments of beech wood char particles of 50 µm to 150 µm in different laboratory reactors (inter alia TGA, FBR and DTR). The resulting reaction rates and activation energies were compared. Their studies widely confirm the findings of Kibria et al. and Baath et al. [4,5]. Following Stoesser et al., the influence of crucible and sample bed diffusion in TGA gasification experiments can be excluded at low reaction temperatures of about 750 –

850 °C, atmospheric pressures and low sample masses (when the sample particles only cover the crucible in a single layer) [2].

In the DTR, a constant sample mass flow and reaction gas volume flow are fed to the reactor. The stationary process allows for analysis of large sample masses. At a given reaction temperature, the reaction gas concentration and the residence time in the hot zone determine the conversion degree at the outlet of the tube. The DTR can be operated at elevated pressure in a temperature range covering the chemical and also the particle diffusion regime by Rossberg and Wicke, ranging from below 900 °C to 1400 °C or more (particle diffusion control) [2,3]. However, the residence time is very short and conversion degrees achieved during experiments at low temperatures in the chemical regime are small [2]. To derive reaction kinetics from the DTR experiments in this case, several sequential runs with the same sample have to be done. At the outlet of the tube, the reaction has to be quenched immediately and the partially converted particles must be separated from the gas stream without fragmentation of those, which is experimentally demanding [2,6]. Dammann et al. [6] investigated the devolatilization of beech wood char from mild pyrolysis at different temperatures in a DTR. The particles were separated in a cyclone at the outlet of the DTR. A comparison of the particle size distribution before and after the heat treatment revealed strong fragmentation of the particles [6]. The reported experiments were conducted in inert atmosphere. For DTR experiments conducted in CO_2 and/or steam, fragmentation has to be expected as well, because the particle structure is additionally weakened due to char consumption.

Comparable to the DTR, in a FBR, reaction temperatures ranging from chemical to particle diffusion regime are possible. The conversion calculation is based on product gas analysis and material balance [7–9]. While the operation of pressurized DTR is well established [10,11], pressurized FBR are rare in literature. As the FBR represents a batch process, changes in product gas concentrations of the FBR process are relevant for determination of reaction kinetics. Investigating gasification kinetics in the FBR therefore faces the problem of backmixing of product gases on their way from the reactor to the gas analyzers. Gövert et al. [7] applied a transfer function based on the convection–diffusion model to describe the changes the concentrations after atmospheric CO_2 gasification respectively combustion underwent on their way to the gas analyzers. This issue will also be further discussed in this work in the context of fixed bed reactors.

Fixed bed reactors allow for continuous record of the whole conversion range of the sample batch ($0 \leq X_C \leq 1$) at elevated pressures and low temperatures in the chemical regime [3]. The carbon conversion is derived from product gas phase analysis and material balancing of C, CO and H_2. The reaction between gas phase and particles in the sample bed causes axial concentration gradients of both reactant and product gas species. These gradients lead to nonuniform reaction conditions in axial direction of the sample bed, with decreasing reactant concentration and increasing product gas inhibition in gas flow direction along the bed. Reduction of the sample bed height (thus sample mass) reduces the changes of the concentrations and therefore leads to more uniform reaction conditions. The differential operation mode is derived from the idea that unlike in a packed bed, in a differential fixed bed, uniform reaction conditions over the sample bed can be assumed. This reactor type will be referred to as dFBR in this paper. As explained above, the range of differential operation depends on the conversion degree of the gaseous reactant. Different threshold degrees of conversions for a gaseous reactant i can be found in literature, ranging from $0.05 \leq X_i \leq 0.1$ [12] to $0.01 \leq X_i \leq 0.03$ [13]. With regard to this ambiguity, the need for a comprehensible definition of the differential operation range is stated. From an experimental point of view, the lower limit of the conversion range is determined by the detection limits of the gas analyzers. The question about a reasonable upper threshold of gas phase conversion in the differential fixed bed will be addressed in this paper.

Another challenge for investigations on reaction kinetics with a differential fixed bed reactor is the non-ideal flow behavior of the gas phase in the tubes, the reactor and the gas analyzers. Axial dispersion in the case of turbulent flow and eventually the parabolic flow profile in the case of laminar flow bring deviations from ideal plug flow behavior [14,15]. Components such as filters, manifolds or cooling traps and temperature and pressure changes on the way to the gas analyzer also cause backmixing and influence the flow profile and therefore the system response behavior [2,7,16,17]. The resulting residence time distribution hence depends on both the construction and choice of process parameters.

2. The differential fixed bed reactor

The differential fixed bed reactor (dFBR) developed and operated at KIT is a top-fed reactor especially designed for differential operation. Reaction kinetics can be investigated at pressures up to 20 bar and temperatures up to 900 °C. The essential components are shown in a flow diagram in Fig. 1.

The plant mainly consists of two strands, the “reactor strand” and the “bypass strand” bypassing the latter one. Two 4-port 2-position valves at the inlet (V1) and outlet (V2) of the two strands allow to switch between the strands. Switching of V1 allows for fast switch between inert gas atmosphere and reaction gas atmosphere at constant temperature and pressure. This design allows for defined reaction conditions in terms of pressure, temperature and gas composition in the reactive zone of the reactor. By actuating V2, either the gas stream from the reactor strand or the gas stream from the bypass strand can be led to the gas analyzers, while the remaining gas stream is led directly to the vent.

2.1. Gas and water dosing system

The applicable gases are carbon dioxide, steam, a calibration gas mixture and argon to one strand and argon to the other strand depending on the position of V1. The volume changing gasification reactions and the removal of condensate influence the product gas volume flow. Therefore, a defined volume flow of nitrogen is added to the product gas at atmospheric pressure before the gas analyzers. By means of this known reference volume flow of N_2, the total volume flow of product gas can be defined (see section 3.2.). The mass-flow controllers (MFC, EL-Flow from Bronkhorst High-Tech B.V.) for the permanent gas species cover a total volume flow range of up to 20 l/min STP for argon and carbon dioxide and 0.5 l/min STP to 5 l/min STP for the gas mixture. All MFCs are calibrated. The calibration line of the N_2 MFC is regularly checked because its preciseness is crucial for the data evaluation (see section 3.2.). The CO_2 MFC was not used in the experiments presented in this work. The type of calibration gas mixture is flexible and chosen depending on the purpose.

The water dosing system comprises a pressurized water tank and a Coriolis Flowmeter (Cori-Flow, Bronkhorst High-Tech B.V.) for measurement of the liquid water flow. The tank can hold up to 5 l of demineralized water. It is pressurized with helium according to the desired reaction pressure and water is led to the Cori-Flow via a dip tube. Helium is chosen because of the low gas absorption into water. Steam generation and mixing of steam and permanent gases happen in the Controlled Evaporation and Mixing unit (CEM, Bronkhorst High-Tech B.V.). It can be operated at temperatures up to 200 °C. The maximum steam partial pressure with respect to this temperature and a surcharge accounting for temperature fluctuations in the CEM is 12.5 bar. All tubes carrying steam are electrically heated at 200 – 250 °C to avoid condensation. The gas phase temperature inside the heated tubes is monitored through several thermocouples.

2.2. Reactor and sample holder

The heated part of the reactor is a 1200 mm long tube of NiCrMo-alloy with an inner diameter of 19.5 mm. An oven made of two half-

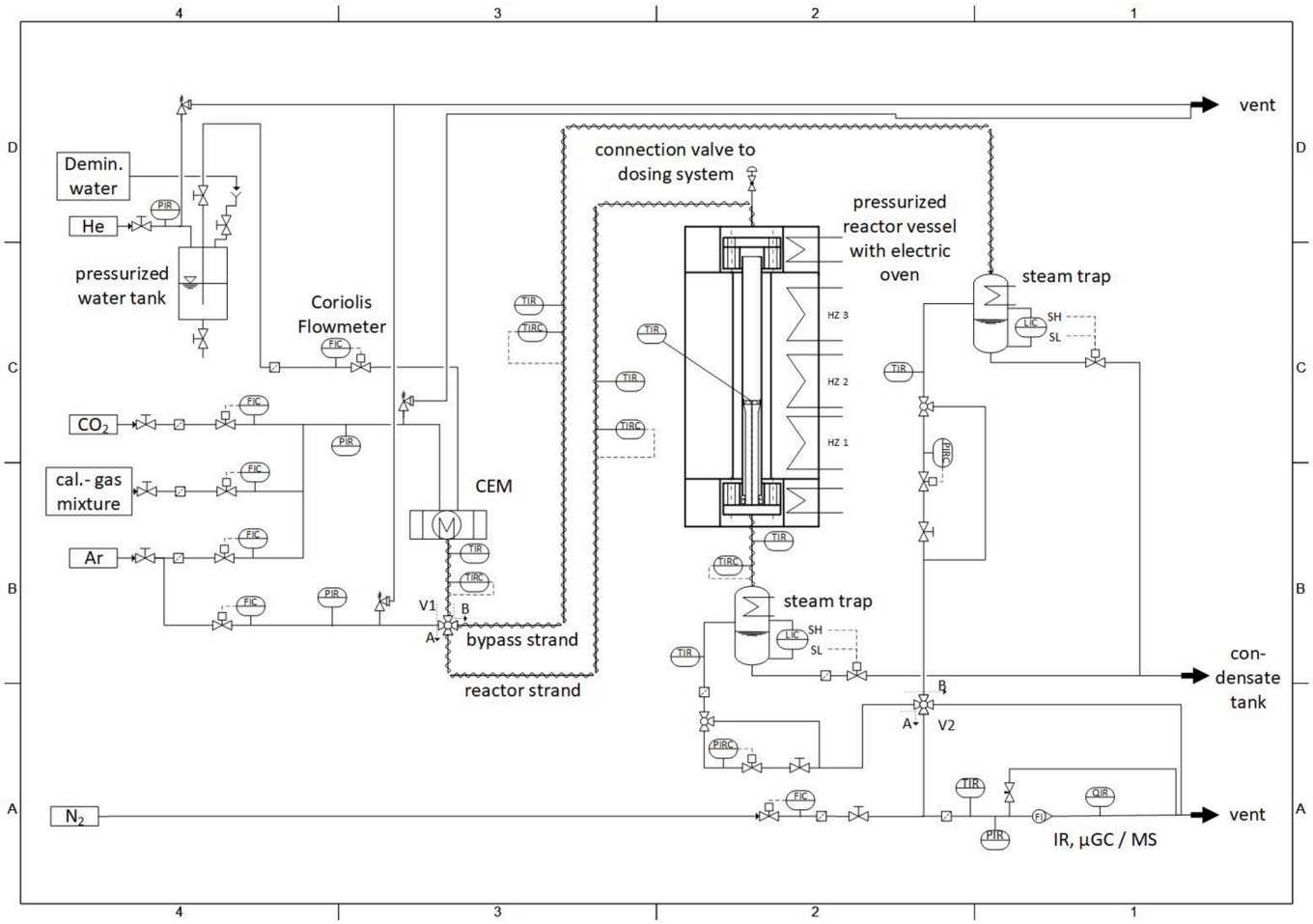

Fig. 1. Simplified flow scheme of the differential fixed bed reactor.

shells heats the reactor tube and ensures isothermal reaction conditions. The temperature can be adjusted by means of three heating zones. A quartz glass sample holder is mounted in the bottom half of the tube. The sample holder consists of a tube (outer diameter: $d_a = 18 \pm 0.5$ mm; wall thickness: $s_w = 1.3 \pm 0.1$ mm) with a fused-in quartz frit and bed of fibrous material on top of the frit. A type K thermocouple is inserted in the center of the tube and the frit to measure the temperature in the sample bed. The design of the sample holder is depicted in Fig. 2 A).

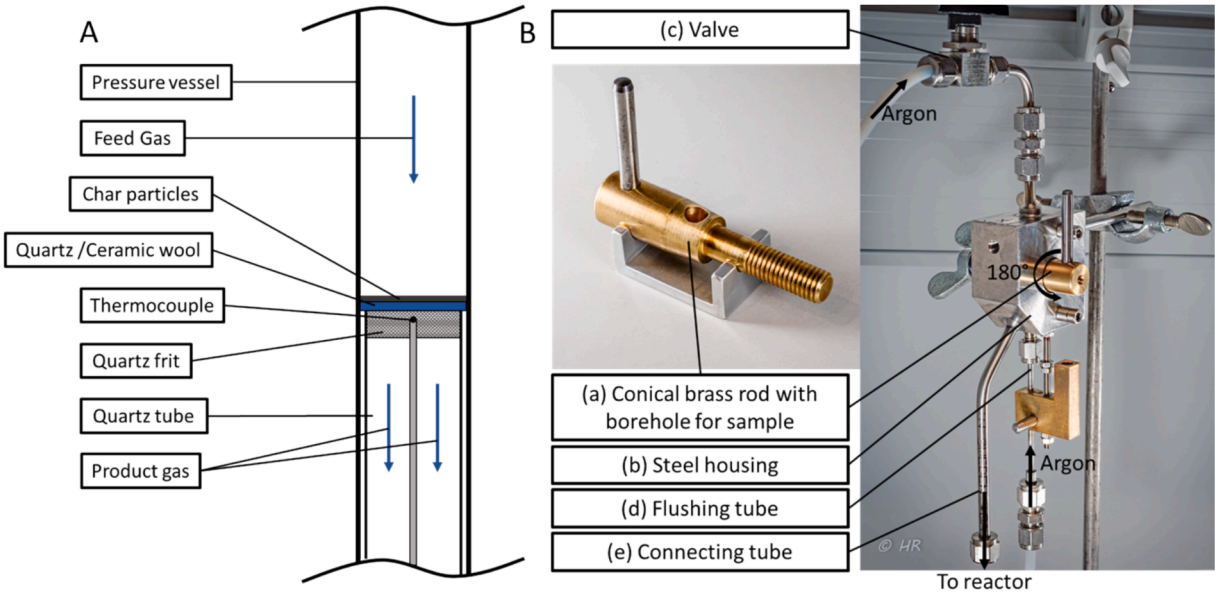

Fig. 2. A) sample holder and B) sample dosing unit (PTFE sealings not shown).

Detailed information on the sample holder is given in the supplementary part A.

2.3. Steam traps and condensate discharge

Further components of both strands are steam traps with automated condensate discharge. The traps consist of a spiral pipe of 4 mm of diameter and 10 m of length cooled with water to 10 °C and a small vessel to collect and discharge the condensate. The collector vessels are designed with low dead volumes to reduce backmixing of the product gases. Two vibration sensors (SITRANS LVL100, Siemens) are mounted in each condensate collector ($V_{total} \approx 120$ ml). When the upper vibration sensor is covered with condensate ($V_{H2O,high} \approx 90$ ml), a solenoid valve downstream of the collector opens and condensate is discharged. As soon as the lower sensor is dry ($V_{H2O,low} \approx 30$ ml), the valve closes. Pictures of the condensate collector are given in the supplementary material F. Remaining water in the collector and the tube upstream the solenoid valve serves as a water seal, preventing gas leakage and product gas accumulation in dead volumes. Thanks to narrow dimensions of the collectors, the water surface is minimized to avoid gas absorption to the condensate, especially for CO_2. Both gas absorption and back mixing in dead volumes would affect the measurement results, thus leading to biased reaction rates. The condensate discharge is monitored and the condensate levels are recorded (high or low) to ensure the condensate discharge.

2.4. Gas analyzers

Upstream V2, back pressure regulators are installed in both strands to control the bypass and reactor pressure and to ensure atmospheric pressure in the gas analyzers. The reference volume flow of nitrogen is added to the dry and atmospheric product gases followed by gas analysis in an infrared photometer for CO determination (IR, URAS 14 AO2020 system, ABB AG) and a micro gas chromatograph (μGC, micro GC 490, Agilent Technologies, Inc.) or mass spectrometer (MS, GAM 400, InProcess Instruments GmbH) for other permanent gas species. The gas analysis has also been subject to optimization. Further details and background information on the choice of the gas analyzers can be found in the supplementary part B. In the presentation of the results, measurements by μGC can be recognized easily by the measurement frequency (e.g. Fig. 7 B), but the analyzer applied will be indicated.

Several filters with 0.5 μm to 7 μm pore width are mounted at different positions to keep small particles from entering delicate components such as the solenoid valves or the gas analyzers (see Fig. 1).

2.5. Sample dosing system

The sample batch of up to 54 mg is carried into the hot reactor and on the fibrous bed through a mobile, argon-flushed dosing system that is connected to a ball valve at the top of the reactor during dosing. The dosing system is depicted in Fig. 2 B). It consists of a conical brass rod with a borehole as sample holder (a) mounted in a steel housing (b) with connecting pipes. The brass rod is sealed tightly against the steel housing (b), eventually using PTFE sealing material. The borehole of the sample holder is flushed with argon for at least 20 min to eliminate remaining oxygen. For the dosing of the sample into the reactor, the reactor has to be at atmospheric pressure and any gas flow through the reactor has to be set off. The connecting tube (e) of the dosing unit is mounted on top of the reactor and the ball valve is opened. The dosing unit is inertised through the reactor for another 20 min. Finally, the sample holder (a) is turned by 180° and the borehole is flushed with argon trough the flushing tube (d) after the valve (c) has been closed. The sample is carried into the reactor and on the sample bed with the argon stream. The ball valve at the top of the reactor is closed again and the dosing unit is removed. Following the dosing procedure, the remaining steps of preparing the experiment (pressurizing and composing the reaction gas atmosphere in the bypass strand, see section 3.1) are carried out immediately.

3. Gasification experiments: procedure, data evaluation and exemplary results

3.1. Experimental procedure

The gasification experiments for this paper were conducted in mixtures of H_2O and argon at total pressures between 5 bar and 20 bar and temperatures in the chemically controlled regime between 810 °C and 870 °C. Technically relevant H_2O partial pressure between 2 bar and 12.5 bar were applied (for entrained flow gasification). The total pressure was selected based on different aspects such as the minimum gas flow for the CEM unit and the gas analyzers.

The selected experimental parameters, weighed sample masses and gas analyzers (IR combined with μGC or MS) are presented in Table 1.

The experiments started with flushing the reactor with an argon volume flow of 0.5 l/min STP and heating up the reactor at atmospheric pressure to the reaction temperature. An argon flow of 0.5 l/min STP was also set for the bypass strand and the tubes in both strands were electrically heated to 200 – 250 °C. The evaporation unit was heated to 200 °C and the pressure in the water buffer tank was set according to the system pressure. The temperature was adjusted by means of the thermocouple mounted in the reactor and the sample holder (see Fig. 2 A). Between 10 mg and 54 mg of sample was weighed and filled into the borehole of the brass cylinder. The sample mass was varied for the verification of differential operation (section 5). The dosing procedure was done as described in section 2.5. The reactor and the bypass strand were subsequently pressurized with argon. The reaction gas atmosphere and pressure were adjusted in the bypass strand. The composition and volume flows of the feed gases were calculated based on ideal gas assumptions and for a uniform gas velocity in the reactor of 10.5 cm/s. Before the start of the reaction, the reaction gas atmosphere in the bypass strand was passed to the gas analyzers for verification of the composition. Afterwards, V2 was switched and the reactor's atmosphere was led to the analyzers. Then, by switching V1 (at the inlet of the reactor), the reaction gas atmosphere was led to the reactor and the sample. The measured concentrations as well as the temperature in the reactor and the tubes were recorded. When the concentrations of CO and H_2 were below 5 – 10 ppm, the experiment was considered terminated. The experiments were repeated 2 – 3 times under the same conditions.

The char used for the gasification experiments presented in this paper was generated by secondary pyrolysis of a primary beech wood char at 1400 °C in a laboratory-scale drop-tube reactor. The primary char originated from mild pyrolysis and still contained 12 wt.-% volatiles [18]. After secondary pyrolysis, the char has been intensively characterized. The results are presented in earlier works of this research group, and the most important properties are summarized in Table 2. [18]. It is assumed that devolatilization does not play a significant role

Table 1
Overview over experimental parameters, sample mass m_0 and gas analyzers.

$T_{Reactor}$	p_{tot}	p_{H_2O}	m_0	Gas analyzer
°C	bar	bar	mg	–
810	5	2	20 ± 0.3	μGC+IR
810, 830, 850, 870	10	5	20 ± 0.8	μGC+IR
810, 830, 850, 870	20	7.5	50 ± 0.7	μGC+IR
810, 830, 850, 870	20	10	50 ± 0.5	μGC+IR
810, 830, 850, 870	20	12.5	50 ± 0.8	μGC+IR / MS+IR
850	15	2	50 ± 4 25 ± 1	MS+IR
870	20	12.5	20 ± 1 11 ± 1	MS+IR

Table 2
Char properties of the secondary char used for the gasification experiments.

Temperature of secondary pyrolysis / °C	1400
Proximate analysis / wt.-%, ad	
Moisture	0.2
Ash content	1.9
Volatiles	2.5
Fixed carbon	95.4
Ultimate analysis / wt.-%, daf	
C	97.2
H	0.2
N	0.7
O (by difference)	1.9
Particle size / µm	50 – 100
Micropore surface area / m^2/g	660

during the gasification experiments because of the high fixed carbon content of 95.4 % and the low volatile content of 2.5 %. As reported in the introduction, film or pore diffusion effects are not expected for this particle size at gasification temperatures below 900 °C. A more detailed explanation of the char generation and further characterization are given in [18]. The char was dried at 105 °C prior to the experiments.

3.2. Evaluation of experimental data: Mass balance and carbon conversion

The carbon conversion during gasification is determined based on product gas analysis and C-,O- and H- balancing and follows the procedure in [19].

Following equation (4) and assuming ideal gas behavior, the flow-rates of all gas components i can be determined with the help of the reference volume flow of N_2 (see section 2.1.):

$$\dot{V}_i = \frac{\dot{V}_{N_2}}{y_{N_2}} \cdot y_i \tag{4}$$

For the carbon conversion X_C, a notional molar flow rate of reaction gases containing converted carbon at time t_i is introduced: $\dot{n}_{C,out}(t_i)$. With $\dot{n}_{C,out}$, the mass of converted carbon at time t_i can be calculated following equation (5).

$$m_{C,conv}(t_i) = m_{C,conv}(t_{i-1}) + \widetilde{M}_C \cdot \dot{n}_{C,out}(t_i) \cdot (t_i - t_{i-1}) \tag{5}$$

The heterogeneous water–gas reaction (r1, equation (1)) and the Boudouard reaction (r2, equation (2)) deliver the product gas species relevant for the determination of $\dot{n}_{C,out}(t_i)$. This leads to the calculation method for the molar flow of converted carbon based on the gas composition determined at time t_i [19,20]:

$$\dot{n}_{C,out}(t_i) = \frac{1}{2}\left(\dot{n}_{CO}(t_i) + \dot{n}_{H_2}(t_i)\right) \tag{6}$$

Based on equations (5) and (6), the total converted carbon mass at time t_i can be expressed by

$$m_{C,conv}(t_i) = m_{C,conv}(t_{i-1}) + \widetilde{M}_C \cdot \frac{1}{2}\left(\dot{n}_{CO}(t_i) + \dot{n}_{H_2}(t_i)\right) \cdot (t_i - t_{i-1}) \tag{7}$$

The total mass of converted carbon $m_{C,gasif}$ corresponds to the converted carbon mass at the end of the gasification experiment.

$$m_{C,gasif} = m_{C,conv}(t_{end}) \tag{8}$$

The time-dependent carbon conversion related to the total mass of converted carbon is given as

$$X_{C,gasif}(t) = \frac{m_{C,conv}(t)}{m_{C,gasif}} \tag{9}$$

The carbon conversion related to the initially weighed carbon mass can also be defined by equation (10).

$$X_{C,weighed} = \frac{m_{C,conv}(t_{end})}{m_{C,0}} \tag{10}$$

3.3. Exemplary results of a gasification experiment

As an example for a gasification experiment and the data evaluation, the product gas species of an experiment at $T_{Reactor} = 830$ °C, $p_{H_2O} = 7.5$ bar and $p_{tot} = 20$ bar as well as the derived conversion $X_{C,gasif}(t)$ (equation (9)) are compiled in Fig. 3.

Based on the conversion $X_{C,gasif}(t)$ the reaction kinetics can be derived as described in the following section.

4. Determination of reaction kinetics from experimental data

The derivation of a reaction rate from the time-course of the conversion $X_{C,gasif}(t)$ requires assumptions regarding the relation between the measured decrease in carbon mass and the reaction rate describing the micro-kinetics of the heterogeneous gasification reactions. This leads to the formulation of particle conversion models describing the conversion rate as the product of a structural term $F(X_{C,gasif})$ and the reactivity R (in s^{-1}).

$$\frac{dX_{C,gasif}}{dt} = R \cdot F(X_{C,gasif}) \tag{11}$$

Based on R, the reaction rate r is determined, e.g. by referencing it to the molar mass of carbon. The unit of r then is $mol \cdot g^{-1} \cdot s^{-1}$.

$$r = \frac{R}{\widetilde{M}_C} \tag{12}$$

A prominent and simple model is the Uniform Conversion Model (UCM), assuming that the reactions occur on reactive centers evenly distributed over the whole particle volume [18,21–23].

$$\frac{dX_{C,gasif}}{dt} = R_{UCM}(1 - X_{C,gasif}) \tag{13}$$

$$X_{C,gasif}(t) = 1 - \exp(-R_{UCM} \cdot t) \tag{14}$$

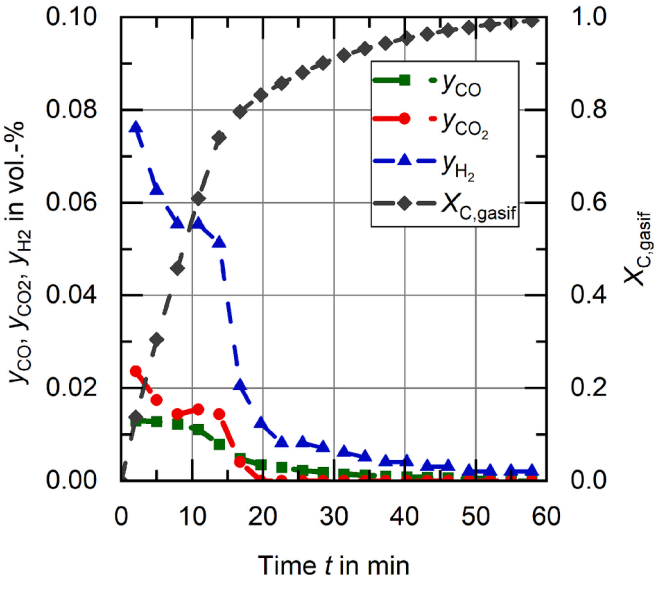

Fig. 3. Product gas composition determined by µGC and IR and derived carbon conversion by mass balance; 50 mg of char were gasified at $T_{Reactor} = 830$ °C, $p_{H_2O} = 7.5$ bar and $p_{tot} = 20$ bar.

The UCM is applicable without additional parameters describing structural aspects and therefore also without introducing unknown degrees of freedom into the conversion model. Equation (14) is fitted to the experimentally derived discrete data for $X_{C,gasif}(t)$ with R_{UCM} as the fitting parameter by least squares method.

On the basis of the experimental and data evaluation procedure presented in sections 3 and 4, solutions to the challenges specific for differentially operated fixed bed reactors will be addressed in the second part of this paper.

5. Verification of the differential operation

5.1. Development of a criterion for differential operation

The idea of differential operation presumes that at low conversion degrees of the gas phase X_i, the changes in gas composition do not influence the reaction kinetics in axial direction of the sample bed. Fig. 4 shows a schematic fixed bed of mass m_{bed} and height H where an arbitrary heterogeneous reaction of $i \rightarrow prod$ takes place. Therefore, the product gas concentration c_{prod} increases and the concentration of reaction gas i, c_i, decreases in axial direction of the sample bed, x.

The assumption, that the reaction kinetics are not influenced by changes in gas composition is always true for a reaction order of $n = 0$. Hence, it is possible to investigate such reaction kinetics with order $n = 0$ without any influence of conversion degree X_i (referring to the gas phase).

To allow for a comparison with reaction orders higher than zero with a characteristic measure, the first Damköhler number Da_I is chosen as the relation between the reaction time scale t_R and the (convective) transport time scale t_τ, i.e. the residence time (equation (15): general definition) [24].

$$Da_I = \frac{t_\tau}{t_R} = t_\tau \cdot k \cdot c_{i,0}^{n-1} \tag{15}$$

This approach is transferred to the case of the differential fixed bed where low Damköhler numbers Da_I thus high convective mass transport compared to the reaction are mandatory. It remains to define a threshold value of Da_I as a criterion for differential operation. The first Damköhler number is generally defined for an irreversible reaction of n-th order following equation (15). For the case of a fixed bed with bed density $\rho_{bed} = m_{bed}/V_{bed}$, bed height H and mass-specific reaction rate constant k_m, the mass balance for gas species i can be formulated as follows:

$$\frac{dn_i}{dt} = -k_m \cdot m_{bed} \cdot c_i^n \tag{16}$$

In a differential section dx of the fixed bed with mass dm_{bed}, the change in reaction gas molar flow $d\dot{n}_i$ respectively concentration $c_i(x)$ is described by equation (17) ($0 \le x \le H$).

$$\dot{n}_i(x) - \dot{n}_i(x - dx) = d\left(\dot{n}_i\right) = \frac{d}{dx}\left(\dot{V}(x) \cdot c_i(x)\right) = -k_m \cdot c_i^n \cdot dm_{bed} \tag{17}$$

As both the Boudouard reaction and the heterogeneous water–gas reaction are volume-changing reactions, the volume flow $\dot{V}(x)$ depends on the conversion degree $X_i(x)$ of the educt gas. Based on the definition of the change in volume flow ε_A (defined for $X_i = 1$) for the plug flow reactor (equation (18)), equation (19) is derived. $y_{i,0}$ is the volume fraction of reactant gas entering the fixed bed, thus in the present case H_2O (or CO_2).

$$\varepsilon_A = \frac{\dot{V}(X_i = 1) - \dot{V}(X_i = 0)}{\dot{V}(X_i = 0)} = \frac{\left(y_{i,0} + 1\right) \cdot \dot{V}_0 - \dot{V}_0}{\dot{V}_0} = y_{i,0} \tag{18}$$

$$\dot{V}(x) = \dot{V}_0 \cdot (\varepsilon_A \cdot X_i(x) + 1) = \dot{V}_0 \cdot \frac{\left(y_{i,0} + 1\right)}{1 + y_{i,0} \cdot c_i(x) \big/ c_{i,0}} \tag{19}$$

Equations (16), (17) and (19) and a dimensionless expression for a modified residence time τ_{mod} (equation (20)) can be summarized in equation (21):

$$V_{bed} \cdot \frac{\rho_{bed}}{\dot{V}_0} = \tau_{mod} \tag{20}$$

$$-k_m \cdot c_{i,0}^{n-1} \cdot \tau_{mod} \cdot d\left(\frac{x}{H}\right) = \left(y_{i,0} + 1\right)\left(\frac{c_{i,0}}{c_i(x)}\right)^n \cdot d\left(\frac{c_i(x)/c_{i,0}}{1 + y_{i,0} \cdot c_i(x) \big/ c_{i,0}}\right) \tag{21}$$

A more detailed derivation of equation (21) can be found in the supplementary part in section E With the definition of the first Damköhler number (equation (15)):

$$-Da_I \cdot d\left(\frac{x}{H}\right) = \left(y_{i,0} + 1\right)\left(\frac{c_{i,0}}{c_i(x)}\right)^n \cdot d\left(\frac{c_i(x)/c_{i,0}}{1 + y_{i,0} \cdot c_i(x) \big/ c_{i,0}}\right) \tag{22}$$

As the modified residence time τ_{mod} and the bed volume V_{bed} are unhandy in the case of a differential sample bed, the first Damköhler number is re-formulated with the measurable variables sample mass m_{bed} and molar flow rate of reactive component $\dot{n}_{i,0}$ at $x = 0$ (equation (23)).

$$-Da_I = -k_m \cdot c_{i,0}^{n-1} \cdot \tau_{mod} = \frac{-k_m \cdot c_{i,0}^n \cdot m_{bed}}{\dot{n}_{i,0}} \tag{23}$$

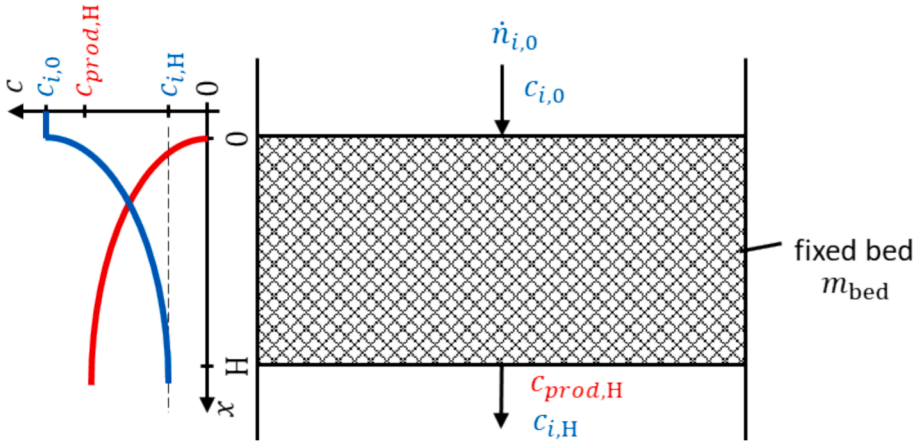

Fig. 4. Schematic fixed bed with changing gas composition upon reaction.

Equation (21) is solved for different reaction orders n and for different reactant gas volume fractions $y_{i,0}$ for both the Boudouard reaction and the heterogeneous water–gas reaction (respecting the change in volume flow based on ε_A). Table 3 shows Da_I for three reaction orders $n = 0$, $n = 0.5$ and $n = 1$ and as a function of $y_{i,0}$. For a given reactant gas composition $y_{i,0}$ respectively $c_{i,0}$, Da_I can be expressed as a function of the ratio of the concentration at the outlet of the bed and the initial concentration of reaction gases $c_{i,H}/c_{i,0}$. This is especially useful as no assumptions about the reaction kinetics of the gas phase conversion or the height of the differential fixed bed have to be made.

Fig. 5 shows Da_I for different $y_{i,0}$ and different reaction orders n. For high concentration quotients $c_{i,H}/c_{i,0}$, Da_I can be fairly approached by Da_I for a reaction order of $n = 0$ (bold black lines in Fig. 5). Hence, it can be assumed that Da_I is independent of the reaction gas concentration and only dependent on the reaction rate constant and the ratio of sample mass and molar reaction gas flow $m_{bed}/\dot{n}_{i,0}$ as the expressions on the left side of the equations in Table 3 can be set equal. By setting a threshold deviation below which the three cases ($n = 0$, $n = 0.5$ and $n = 1$) are considered as equal and determining the corresponding ratio $c_{i,H}/c_{i,0}$, the criterion is derived. In this work, a deviation of 2.5 % was set and the corresponding ratio $c_{i,H}/c_{i,0}$ and Da_I are indicated by red lines in Fig. 5.

Fig. 5 reveals that the Damköhler numbers Da_I corresponding to the deviation of 2.5 % of $c_{i,H}/c_{i,0}$ lie between 0.05 and 0.088 and the absolute values of $c_{i,H}/c_{i,0}$ lie between 0.904 and 0.905. For the sake of simplicity, a concentration quotient of $c_{i,H}/c_{i,0} \geq 0.9$ is chosen as the criterion for differential operation.

5.2. Application of the criterion to experimental data

In the preceding section, a threshold value for the concentration quotient of reaction gas i (in our case H_2O) leaving ($c_{i,H}$) and entering ($c_{i,0}$) the differential fixed bed $c_{i,H}/c_{i,0}$ was determined as a criterion for differential operation. For $c_{i,H}/c_{i,0} \geq 0.9$, the fixed bed is operated differentially. This allows to determine which molar fractions of reaction gas i at the outlet of the differential fixed bed is at least necessary to fulfill the criterion for differential operation for the experiments conducted. Thereby, also the maximum molar fractions of product gases tolerated for differential operation can be derived. These threshold product gas fractions are calculated using the volume flows in the experiments at different H_2O partial pressures of 5, 7.5, 10 and 12.5 bar.

In the reactor, part of the CO reacts with H_2O molecules to form H_2 and CO_2 or vice versa. As the H_2-concentration increases correspondingly to the decrease of the CO-concentration (or vice versa), it is suitable to consider the sum of the molar fractions of the product gases CO and H_2. A detailed derivation of the calculation steps is given in supplementary material E.

Fig. 6 summarizes the derived calculated threshold values of $\left(y_{CO} + y_{H_2}\right)_{H,calc}$ for $c_{i,H}/c_{i,0} = 0.9$ (solid lines) and the sum of the maximum measurement values $\left(y_{CO} + y_{H_2}\right)_{H,exp}$ (data points). The measured fractions $\left(y_{CO} + y_{H_2}\right)_{H,exp}$ are at least one order of magnitude below the calculated threshold concentrations. So the criterion for differential operation is exceeded in none of the experiments, although the weighed sample mass varied (see Table 1).

In Fig. 7, the conversion curves $X_{C,gasif}(t)$ for gasification experiments with different steam partial pressures, temperatures and sample masses from 10 mg to 50 mg (see Table 1) are compared to verify the criterion. Dotted data were gained from gas analytics with μGC and IR, lines indicate quasi-continuous measurements with MS and IR. The time course of the carbon conversion and therefore the conversion rate was the same for all sample masses. The experiments were also reproducible for both gas analyzers (μGC and MS, Fig. 7 B)). The reproducibility with respect to the sample masses is only possible when the fixed bed reactor is operated differentially, as otherwise, decreasing educt gas concentrations and increasing product gas concentrations would influence the particle conversion rate in axial direction of the fixed bed. Consequently, the observed conversion rate would lead to packed bed kinetics and therefore depend on the sample mass. By means of Fig. 7, it can be seen that the criterion developed in this paper can be used to assess differential operation and that sample masses of 10 mg to 50 mg of biomass char are suitable for differential operation of the dFBR.

6. Description of the system response behavior with the axial dispersion model

The response of a system to a perturbation can be described by convolution of the perturbation with a system-specific weight function (corresponding to the transfer function in the Laplace region).

For a flow-through system (e.g. laboratory reactor and periphery), an infinitesimal volume element entering the system will remain in the system according to the residence time distribution $E(t)$. It follows that for a pulse of a component i with a concentration $c_{i,in}(t = 0)$, the concentration at the outlet, $c_{i,out}(t)$, can be described by the convolution integral of the entering concentration $c_{i,in}(t)$ with the residence time distribution function $E(t)$ (the weight function, equation (24)).

$$c_{i,out}(t) = \int_0^{t'} c_{i,in}(t - t') \bullet E(t')dt' \tag{24}$$

Notions used to describe the system response behavior are summarized in Fig. 8 showing the response of a system to a concentration step at time $t = 0$ (concentrations are normalized).

The system response time is defined as the time between the input signal and the first response signal (Fig. 8). In the case of short system response times and very narrow residence time distributions (small spread of $E(t)$), the influence of the system response behavior might be neglectable. Stoesser et al. [2] assigned the response control to domains

Table 3
Da_I for different reaction orders and reaction gas compositions.

Reaction order	Da_I
$n = 0$	$Da_I = \frac{k_m \cdot m_{bed}}{\dot{n}_{i,0}} = -\frac{\left(\frac{c_{i,H}}{c_{i,0}} - 1\right)}{1 + y_{i,0}\frac{c_{i,H}}{c_{i,0}}}$
$n = 0.5$	$Da_I = \frac{k_m \cdot m_{bed} \cdot \sqrt{c_{i,0}}}{\dot{n}_{i,0}} = -\left(1 + y_{i,0}\right) \cdot \left[\frac{arctan\left(\sqrt{\frac{1}{y_{i,0}}}\right) - arctan\left(\sqrt{\frac{1}{y_{i,0}\frac{c_{i,H}}{c_{i,0}}}}\right)}{\sqrt{y_{i,0}}} + \frac{\sqrt{\frac{c_{i,H}}{c_{i,0}}}}{1 + y_{i,0}\frac{c_{i,H}}{c_{i,0}}} - \frac{1}{(1 + y_{i,0})}\right]$
$n = 1$	$Da_I = \frac{k_m \cdot m_{bed} \cdot c_{i,0}}{\dot{n}_{i,0}} = -(1 + y_{i,0}) \cdot \ln\left(\frac{\left(1 + y_{i,0}\right)\frac{c_{i,H}}{c_{i,0}}}{1 + y_{i,0}\frac{c_{i,H}}{c_{i,0}}}\right) + \frac{y_{i,0}\left(1 - \frac{c_{i,H}}{c_{i,0}}\right)}{1 + y_{i,0}\frac{c_{i,H}}{c_{i,0}}}$

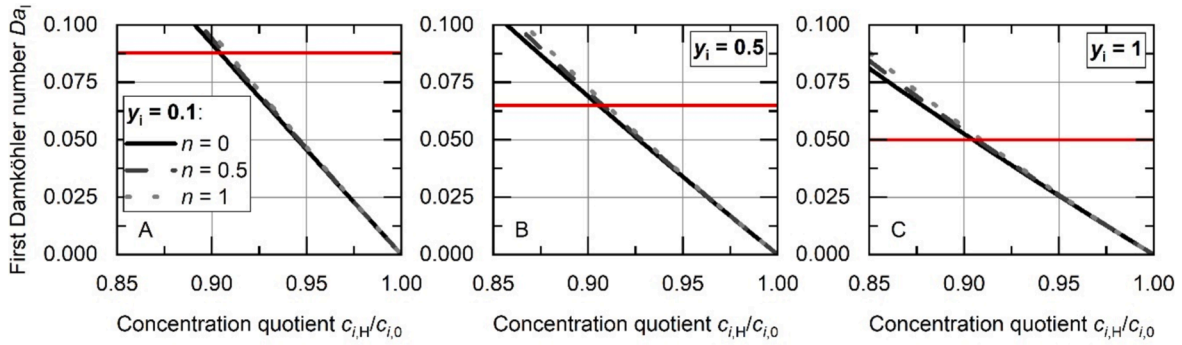

Fig. 5. First Damköhler numbers Da_I as a function of the concentration quotient $c_{i,H}/c_{i,0}$ for different reaction orders and different reaction gas mole fractions A) $y_{i,0} = 0.1$, B) $y_{i,0} = 0.5$ and C) $y_{i,0} = 1$; red line indicates where $c_{i,H}/c_{i,0}$ deviates by less than 2.5 %. (For interpretation of the references to colour in this figure legend, the reader is referred to the web version of this article.)

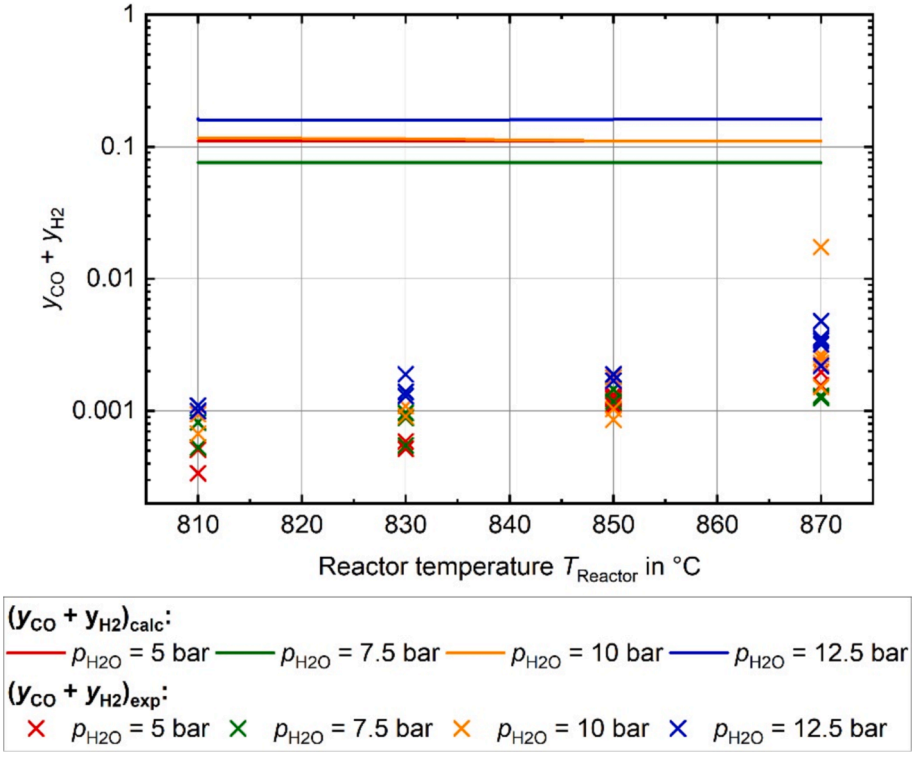

Fig. 6. Derived sum of maximum concentrations $(y_{CO} + y_{H_2})_{H,calc}$ for $c_{i,H}/c_{i,0} = 0.9$ and actual sum of the measurement values $(y_{CO} + y_{H_2})_{H,exp}$ for three experimental series at $p_{H_2O} = 5\ bar$, $p_{H_2O} = 7.5\ bar$,$p_{H_2O} = 10\ bar$ and $p_{H_2O} = 12.5\ bar$ and reactor temperatures from $T_{Reactor} = 810\ °C$ to $T_{Reactor} = 870\ °C$.

where the orders of magnitude of the reciprocal reactivity $1/R$ and the system response time correspond to one another. If the magnitude of $1/R$ is similar to the magnitude of the response time, ignoring the system response behavior would lead to misinterpretation of the experimental data. However, this approach does not include the residence time distribution function $E(t)$ and therefore, does not consider a significant part of the system response behavior.

In this work, the residence time distribution function $E(t)$ is included into the evaluation of reaction kinetic experiments following equation (24), to assess the influence of the system response behavior and to derive reaction kinetics from experimental data corrected for the system response behavior. For this purpose, two issues have to be addressed. First, for evaluation of experimental data based on signal analyses that undergo transformation on their way to the analyzing unit, the system-specific function $E(t)$ has to be determined [16,25]. And second, a method to derive the original perturbation in the sample bed based on the system response and $E(t)$ has to be developed.

6.1. A model for the system specific response function

To solve the first problem, it is suitable to investigate distinct perturbation functions [16]. The normalized response to an ideal pulse function (Dirac impulse) corresponds to the residence time distribution $E(t)$. The normalized response to a step function (Heaviside function) corresponds to $F(t)$, the primitive of $E(t)$. The mathematical formulation of $E(t)$ may be derived from different models such as the tank-in-series-model or the axial dispersion model [25]. In the case of rather complex apparatuses where the gas flow passes through different temperature and pressure regimes or where part of the gas phase is condensed (e.g. steam gasification experiments), the gas velocity changes continuously. The axial dispersion model has found wide application as a semi-empirical model to holistically describe the flow behavior of such systems [7,8,14,26–28]. In contrast, the tank-in-series model requires definition or adjustment of the number of cells in each velocity regime. In the laboratory plant investigated here, this adjustment could not be

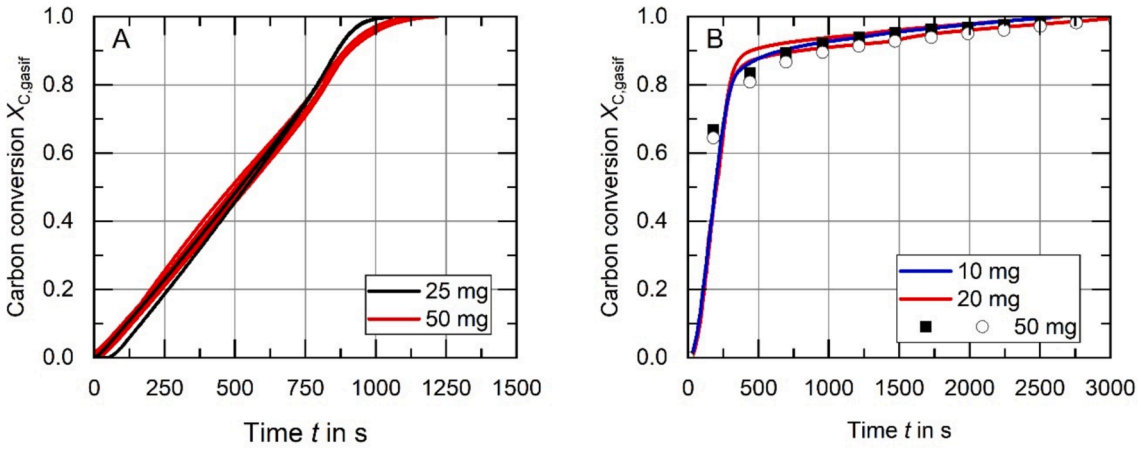

Fig. 7. Gasification experiments with different sample masses: A) $T_{Reactor} = 850\ °C$, $p_{tot} = 15\ bar$, $p_{H_2O} = 2\ bar$, $m_{char} = 50\ mg$ and $m_{char} = 25\ mg$; and B) $T_{Reactor} = 870\ °C$, $p_{tot} = 20\ bar$, $p_{H_2O} = 12.5\ bar$, $m_{char} = 10\ mg$, $m_{char} = 20\ mg$ and $m_{char} = 50\ mg$ (dotted data were gained from gas analysis with μGC).

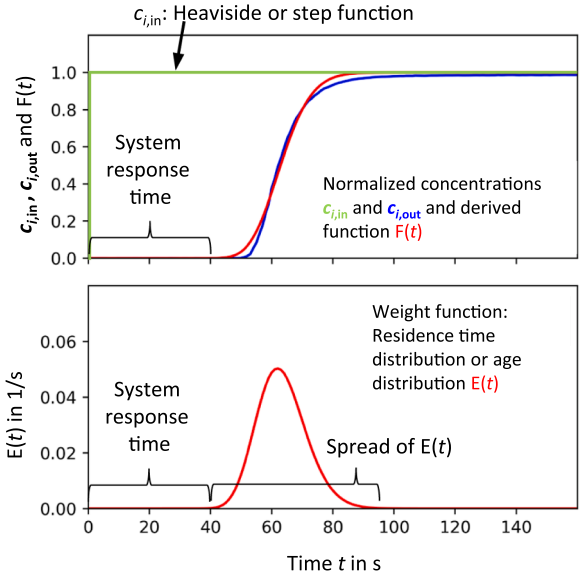

Fig. 8. Notions used to describe the system response behavior.

verified by measurements after each velocity regime. Therefore, the axial dispersion model is chosen for the description of the system response.

The basis of the axial dispersion model is the one-dimensional convection–diffusion-equation with c_i being the concentration of a tracer component i as a function of time t and axial coordinate z [16]. $\partial c_i/\partial t$ depends on the axial dispersion coefficient D_{ax} and the axial velocity u (equation (25)).

$$\frac{\partial c_i(t,z)}{\partial t} = D_{ax}^2 \frac{\partial^2 c_i(t,z)}{\partial z^2} - u \cdot \frac{\partial c_i(t,z)}{\partial z} \tag{25}$$

The dispersion coefficient D_{ax} is a measure for the spreading process with large values of D_{ax} indicating rapid spreading and a wide spread of E(t) and low values indicating slower spreading and a narrow spread of E(t) (see Fig. 8). It is of the same dimensions as the molecular diffusion coefficient (m^2/s). The dispersion is dependent on the axial flow velocity, the molecular diffusion coefficient and the flow properties that can be summarized in the Bodenstein number Bo.

$$Bo = \frac{u_Z \cdot L}{D_{ax}} \tag{26}$$

The Bodenstein number can be calculated based on the axial Péclet number Pe_{ax} without knowledge of the axial dispersion coefficient. The axial Péclet number in turn relies on the Reynolds and Schmidt number in a flow-regime dependent manner [15,16,24,25,29].

$$Pe_{ax} = \frac{u_Z \cdot d_R}{D_{ax}} \tag{27}$$

$$Pe_{ax} = f(Re, Sc) \tag{28}$$

Laplace-transformation and solution of the differential equation (25) with the boundary conditions

$$c(0,0) = c_0 \tag{29}$$

$$c(0,z) = 0 \tag{30}$$

$$c(0,L) = 0 \tag{31}$$

$$\lim_{t\to\infty} c(t,z) = c_0 \tag{32}$$

$$0 \le z \le L \tag{33}$$

results in function F(t) (equation (34)) [16].

$$F(t) = \frac{c(t,L)}{c_0} = \frac{1}{2}\left\{ \operatorname{erfc}\left(\frac{f_1 - 2f_2 t}{2\sqrt{t}}\right) + \exp(2f_1 f_2) \cdot \operatorname{erfc}\left(\frac{f_1 + 2f_2 t}{2\sqrt{t}}\right) \right\} \tag{34}$$

The parameters f_1 and f_2 can be experimentally derived from step experiments. For a simple, model like system as described by Abad et al. [16] (one straight tube of length L, constant velocity u, temperature and pressure) the parameters f_1 and f_2 are defined as

$$f_1 = \frac{L}{\sqrt{D_{ax}}} \tag{35}$$

$$f_2 = \frac{u}{2\sqrt{D_{ax}}} \tag{36}$$

It will be seen later on that also for more complex systems, the parameters strongly correlate due to their common denominator, the square root of the axial dispersion coefficient.

6.2. *Validity of the axial dispersion model*

The axial dispersion model holds for turbulent flows where the dispersion can be explained by turbulences and where the residence time distribution follows a Gaussian Curve (mixing processes of

stochastic nature) [24,25]. It is often also applied more generally to describe the deviation from an ideal plug flow in other flow regimes, but the validity of the axial dispersion model has to be checked in these cases [14,16,29]. Therefore, the flow regimes in the reactor and the pipes were analyzed based on the Reynolds and eventually the Bodenstein number.

For this first estimation, the influence of reactor inlet and outlet, filters or elbows in the pipes were ignored. The results will be summarized briefly here. More detailed results are available in the supplementary material C. Temperatures between ambient temperature (293.75 K) and maximum temperature (573.15 K for the pipes and 1173.15 K for the reactor) and pressures up to 20 bar were considered. A turbulent flow regime with Bodenstein numbers $Bo > 100$, thus ideal plug flow, was found for the connecting pipes following [24]. The flow regime in the reactor is laminar with Reynolds numbers of $Re < 400$ for a mixture of 50 % CO_2 or H_2O and 50 % Argon. Hence, the validity of the axial dispersion model for the reactor pipe has to be checked.

For this purpose, different methods are proposed in literature to exclude radial concentration gradients for laminar flows in long pipes [14,24,25,29]. For example, Boskovic uses a comparison of the vessel geometries and time scales for convective and diffusive mass transport proposed by Ananthakrishnan et al., Reejhsinghani et al. and Ekambara et al. [14,15,30,31]. In the work at hand, the Fourier number for radial mass transport as the ratio between convective (τ) and diffusive (t_D) mass transport $Fo = \tau/t_D$ was determined (equation (37)) [24].

$$Fo = \frac{\tau}{t_D} = \frac{\tau \cdot D_m}{r^2_{channel}} \tag{37}$$

In the case of laminar flow regime, three cases can be distinguished.

In the first case, $t_D \ll \tau$, thus $Fo = \tau/t_D \rightarrow \infty$: diffusion is faster than convection, so due to strong radial cross-mixing an ideal plug flow can be assumed and the axial dispersion model can be applied.

In the second case, $t_D \gg \tau$, thus $Fo = \tau/t_D \rightarrow 0$: diffusion is slower than convection, so little radial cross-mixing takes place and the flow profile is parabolic (fully segregated), so the axial dispersion model cannot be applied.

In the third case, $t_D \approx \tau$, thus $Fo = \tau/t_D \approx 1$: The flow profile is partially segregated. In this regime, the dispersion model can be applied following [24].

The molecular dispersion coefficient D_m and the Fourier number (equation (37)) were determined for the reactor pipe for different temperatures and pressures according to the experimental matrix. D_m was calculated following [32]. Depending on the reactor temperature and pressure, diffusion coefficients $7.73 \cdot 10^{-6}\ m^2/s \leq D_m \leq 2.83 \cdot 10^{-4}\ m^2/s$ and Fourier numbers $0.83 \leq Fo \leq 35$ were determined for a mixture of 50 % CO_2 or H_2O and 50 % Argon. More detailed results are available in the supplementary material C. Consequently, a partially segregated flow profile, eventually with strong cross-mixing can be assumed and the application of the axial dispersion model is feasible.

Uncertainty remains with regard to the influence of in- and outlet of the reactor, the heat-up of the gas phase in the reactor as well as the sample holders and the steam traps on the step responses. Generally, installations in tubes as the sample holder should not restrict the applicability of the model [25]. It will be tested in the following section if the axial dispersion model can holistically describe the system response behavior including the influence of sample holder, reactor outlet and steam traps. Analysis of the influence of the reactor inlet on the experimentally derived system responses was carried out with the clear result that the influence is neglectable (see supplementary material D).

6.3. Deriving the particle conversion from the observed conversion

The second problem was to develop a method to derive the original perturbation in the sample bed based on the system response and $E(t)$. Addressing this by deconvolution of equation (24) to derive $c_{i,in}(t)$ brings several difficulties. As the experimental measurement of $c_{i,out}$ results in discrete data points, the mathematical formulation of equation (24) consists of a matrix E and vectors for C_{in} and C_{out}. C_{in} describes the (unknown) perturbation resulting from heterogeneous reaction in the sample bed.

$$C_{out} = E \bullet C_{in} \tag{38}$$

The matrix usually results from experimental measurements with equidistant time steps and will contain a certain amount of noise [7,26,33]. Deconvolution would amplify the noise, furthermore, the inversion of E (E^{-1}) is an ill-posed problem without a direct mathematical solution [7,14,26,33]. It is however possible to fit the result of the convolution of C_{in} with E to the result C_{out}, if a model is given to calculate the elements of the vector C_{in}. As no model for C_{in} is available, the particle conversion in the sample bed $X_{part}(t)$ is considered as the perturbation instead. The observed conversion X_{obs} directly calculated from the gas analysis according to equation (9) in section 3.2. is regarded as discrete values of the system response. Hence, X_{part} is a series of pulse perturbations and results in X_{obs} by convolution with E. The particle model (Uniform Conversion Model – UCM, equation (14)) is used as a model for X_{part} with the reactivity R_{UCM} being the fitting parameter in equation (39).

$$X_{obs}(t) = \int_0^t X_{part}(t') \bullet E(t - t')dt' = \int_0^t X_{part}(t - t') \bullet E(t')dt' \tag{39}$$

As mentioned in the introduction, a comparable approach can be found in Gövert et al. [7]. Evaluation routines were established for both fitting of the experimental data of the step response experiments to equation (34) and for processing the reaction kinetic data to the convoluted UCM model by minimizing the least squares (equation (39)). Hereafter, this evaluation method will be called UCM-C (UCM-convolution) to distinguish it from the sole application of the UCM (equation (14)).

6.4. Experiments for determination of a weight function for the system specific response

Experiments with concentration steps were performed as they are experimentally more feasible than concentration pulse experiments. Since axial flow velocity, the molecular diffusion coefficient and the flow properties that can be summarized in the Bodenstein number influence the dispersion [15,16,25,29], the following parameters were considered for the investigations on the system response in the laboratory plant: temperature, pressure and gas composition. Experiments were carried out at temperatures between 810 °C and 870 °C and for total pressures from 5 bar to 20 bar according to the conditions of the gasification experiments. For investigations on the reactor strand, volume flows were adjusted to the required velocity of 10.5 cm/s in the reactor as for the gasification experiments (see section 3.1.). Calculations were based on ideal gas assumptions. Table 3 summarizes the parameter variation of the step response experiments.

A gas mixture containing approximately 500 ppm CO, H_2 and CH_4 (each) besides larger concentrations of CO_2 (30 vol.-%), N_2 and Ar was used as a tracer gas. The investigation of the system response behavior was supposed to account not only for the steam experiments presented in this paper but also for experiments with CO_2 or steam and CO_2. Therefore, the composition of the gas mixture was chosen as a composition of dry gases occurring in the product gases of experiments with steam and/or CO_2. The gas mixture was combined with different amounts of steam and argon (see Table 4). The CO concentration was quasi-continuously recorded in the IR gas analyzer (one record per second). Depending on the desired gas composition, the volume flows of the gas mixture, argon and steam were set. The normalized CO-concentrations were considered for the evaluation and for the comparison between experiments of different parameter sets.

Table 4
Parameter variation for step response experiments to determine the weight function of the laboratory plant (the gas mixture contains approximately 500 ppm CO, H_2 and CH_4 (each) besides larger concentrations of CO_2, N_2 and Ar).

Gas composition for series	$y_{\text{gas mixture}}$	y_{Ar}	y_{H_2O}
A	0.5	0.5	0
B	0.25	0.5	0.25
C	0.4	0.2	0.4
Temperature $T_{Reactor}$ in °C	810, 830, 850, 870		
Total pressure p_{tot} in bar	5, 10, 15, 20		
Velocity in the reactor tube u_{gas} in cm/s	10.5		
Repetition	2 – 3 times		

To prepare the experiment, the reactor was heated up as described for the gasification experiments in section 3.1. In the case of step experiments with steam, the tubes were heated as well. For step response experiments through the reactor strand, a volume flow carrying the tracer gas, argon and eventually steam was led through the bypass strand and directly to the vent. Then, V1 at the inlet side of the reactor was switched and the gas flow carrying the tracer was led through the reactor and to the gas analyzer. The position of V1 and V2 and therefore the starting time of the step experiments was recorded. The increase of the CO-concentration was observed. When the concentration stayed constant for at least 30 s, the experiment was considered terminated. Before and after each measurement, all tubes and the gas analyzer were flushed with argon until no tracer gas could be detected anymore. Equation (34) was fitted to the normalized CO-concentrations with the least squares method to determine the parameters f_1 and f_2 as fitting parameters.

6.5. Results of the step response experiments

The step responses of the reactor line were compared for different temperatures, pressures and gas compositions. The step responses at 810 °C and different steam partial pressures are depicted in Fig. 9. The influence of the reactor temperature for a total pressure of 15 bar is exemplarily shown in Fig. 10. The line styles (solid line, dashed line, dotted line) represent the repeated experiments at the same conditions. No or minor influence of total pressure or reactor temperature on the step response can be stated by means of Figs. 9 A) and 10, respectively. From comparison of Fig. 9 A), B) and C), the major influence can be assigned to the steam content in two ways. On the one hand, the response behavior is more delayed for higher steam contents. On the other hand, while the responses of the experiments with 0 % H_2O are nearly congruent, this is not given for increasing steam content

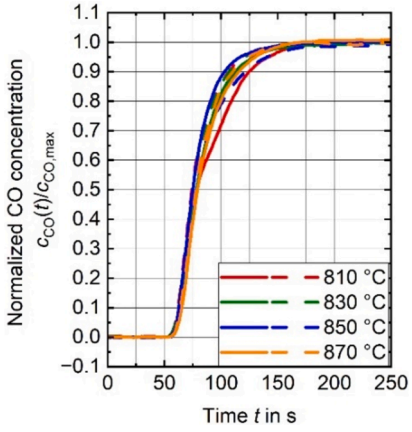

Fig. 10. Step responses of the reactor at different temperatures $810\ °C \leq T_{Reactor} \leq 870\ °C$, $y_{H_2O} = 0.25$ and a total pressure $p_{tot} = 15\ bar$.

especially at higher values of $c_{CO}(t)/c_{CO,max}$.

This delay and diversification are most probably attributed to the condensation of steam in the coils of the steam straps. With increasing steam content, more volume of the pipe is occupied by condensate droplets or a condensate film. Larger droplets can occur, blocking parts of the pipe. It is likely that this leads to an unsteady gas volume flow, resulting in the unspecific diversification of the response curves at high steam contents. When evaluating the derived weight functions for evaluation of reaction kinetic data, the influence of this diversification of the response curves on the reaction rates resulting from UCM-C evaluation will be discussed (section 6.7.1.).

A summary of the influence of temperature, pressure and steam content on the step response in the reactor is also given by means of Fig. 11. Here, the time until the normalized CO concentration reached 0.5 is plotted against the total pressure (Fig. 11 A) and the reactor temperature (Fig. 11 B). The large influence of the steam content and the low influence of temperature and pressure become apparent once again.

The experiments at $y_{H_2O} = 0.25$ were carried out after evaluation of the experiments at $y_{H_2O} = 0$ and $y_{H_2O} = 0.4$, because the strong influence of the steam content was observed. As it was already clear that the reactor temperature did not influence the system response curves, only two temperatures (810 °C and 870 °C) were investigated.

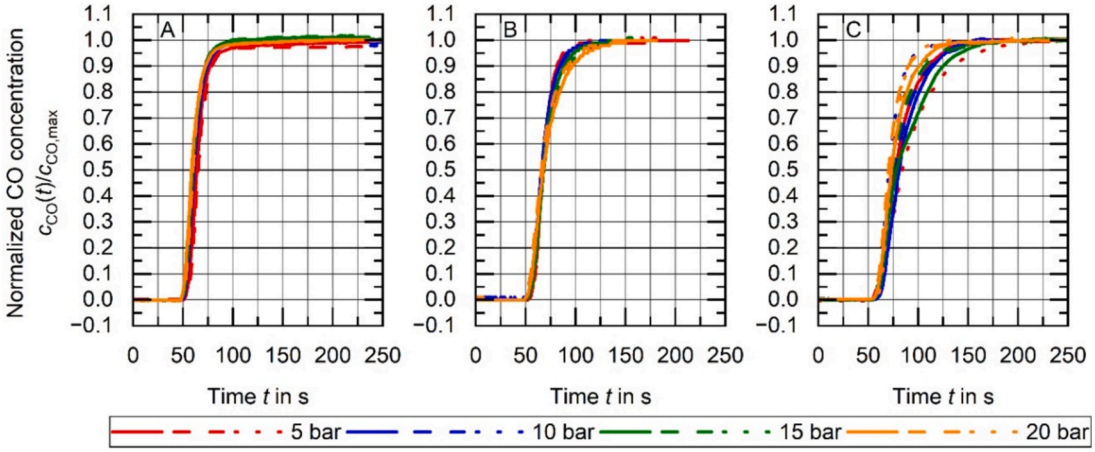

Fig. 9. Step responses of the reactor line at $T_{Reactor} = 810\ °C$, varying total pressures ($5\ bar \leq p_{tot} \leq 20\ bar$) and increasing steam contents: A) $y_{H_2O} = 0$, B) $y_{H_2O} = 0.25$, C) $y_{H_2O} = 0.4$.

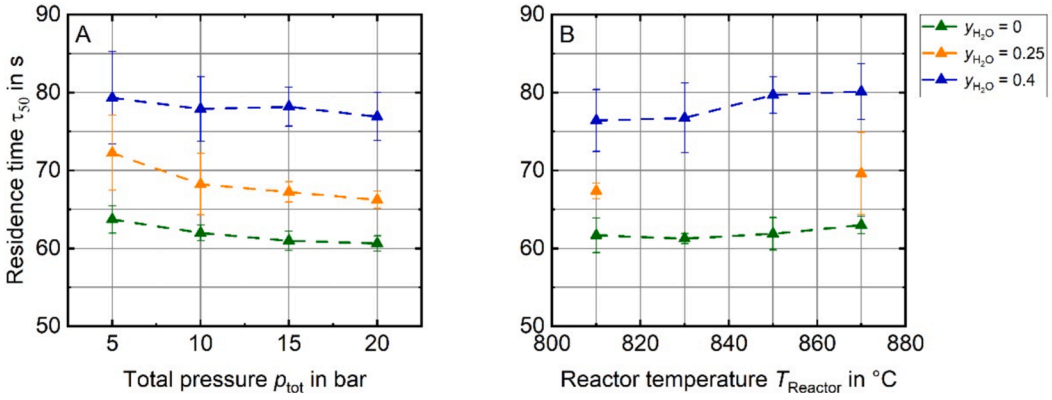

Fig. 11. Residence time until 50 % of the maximum CO concentration is reached: A) for different total pressures, B) for different temperatures in the reactor strand with increasing steam contents: green: $y_{H_2O} = 0$, orange: $y_{H_2O} = 0.25$, blue: $y_{H_2O} = 0.4$. (For interpretation of the references to colour in this figure legend, the reader is referred to the web version of this article.)

6.6. Application of the weight function based on the axial dispersion model to step experiments

The parameters f_1 and f_2 of equation (34) were fitted to the normalized step responses. The region of very low CO concentrations (below 10 ppm) were not included in the evaluation because of the limitations of the linear measuring range of the photometer. This corresponds to the first 4 – 5 s of the response curve respectively the region up to 5 % of the maximum CO concentration. Examples of the fitting results for step responses recorded at $T_{Reactor} = 870$ °C, $p_{tot} = 15$ bar and different steam contents are given in Fig. 12. With increasing steam content, the residence time distributions become broader. It can be seen that especially at high steam contents, the fit loses some precision. As discussed in the preceding section, this inaccuracy results from the condensation in the steam traps.

To assess the influence of the process conditions (temperature, total pressure, steam content) on f_1 and f_2, a correlation matrix (Table 5) was determined. Parameters f_1 and f_2 were averaged for step response experiments with the same temperature, total pressure and steam content. As already expected based on the observations of the step experiments, the correlation between the parameters related to the steam content is strong. Furthermore, a strong correlation also exists between f_1 and f_2. This is conceivable with regard to the definition of f_1 and f_2 from the convection–diffusion model. Both parameters have the square root of the axial dispersion coefficient as common denominator (equations (35) and (36).

The correlation of f_1 and f_2 with the steam content can be described by a linear relation. Fig. 13 shows the linear fit of f_1 and f_2 to the steam content and equations (40) and (41) summarize the linear fitting results. Both parameters decrease with increasing steam content. Thus, high parameters of f_1 and f_2 correspond to steep response curves and narrow residence time distributions whereas lower parameters correspond to broad residence time distributions.

Table 5
Correlation matrix of reactor temperature, total pressure, steam content and parameters f_1 and f_2.

	$T_{Reactor}$	p_{tot}	y_{H_2O}	f_1	f_2
$T_{Reactor}$	1,00				
p_{tot}	0,00	1,00			
y_{H_2O}	−0,03	0,03	1,00		
f_1	0,09	−0,10	−0,69	1,00	
f_2	0,06	−0,05	−0,79	0,99	1,00

$$f_1\left(y_{H_2O}\right) = 92.891 - 78.265 \cdot y_{H_2O} \quad (40)$$

$$f_2\left(y_{H_2O}\right) = 0.7459 - 0.8735 \cdot y_{H_2O} \quad (41)$$

The considerable deviations of the response curves at higher steam contents result in large error bars for the fitting parameters f_1 and f_2 in Fig. 13. As announced previously, the reactivity determined with the minimum and maximum parameters for f_1 and f_2 (indicated by error bars in Fig. 13) will be compared to the reactivity determined with the

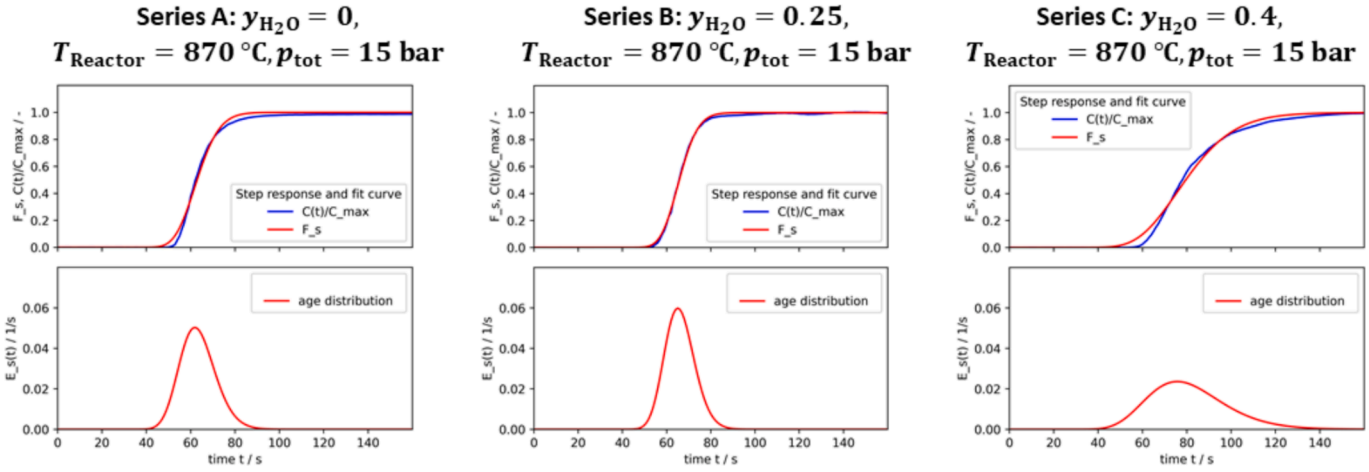

Fig. 12. Fitting results of the step response model equation (34) to experiments.

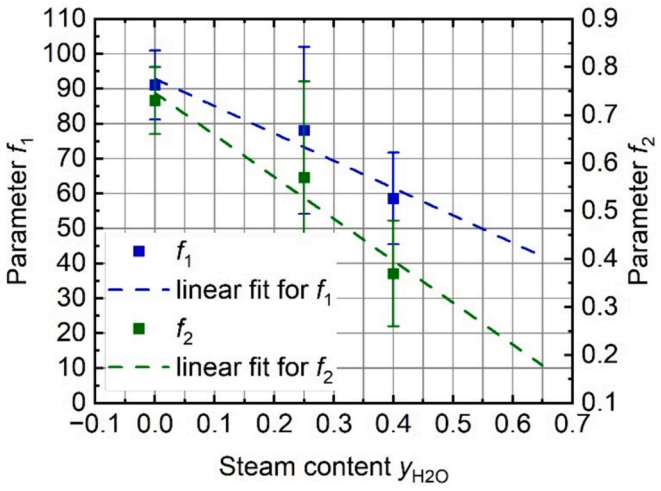

Fig. 13. Linear fit of f_1 and f_2 to the steam content y_{H_2O}: data points: average values, error bars: minimum and maximum values.

parameters derived from the linear fit to assess influence of these diversifications of the response curves on the reaction rates resulting from UCM-C evaluation (section 6.7.1.).

6.7. Evaluation of gasification experiments with the modeled system response

Schneider et al. [19] restricted the conversion range of the experimental data to $0.2 \leq X_{C,gasif} \leq 0.5$ for calculation of the reaction kinetics. The authors argued that the influence of the effects of gas switch at the start of the experiments had to be excluded in deriving reaction kinetics. After investigating the flow regimes in the different sections of the laboratory plant and considering the response behavior of the reactor, it can be stated that these concerns do not hold for the differential fixed bed reactor and the data evaluation method presented here. Therefore, for the present work, conversion ranges of $0 \leq X_{C,gasif} \leq 0.8$ were considered for the UCM-C evaluation and also for the UCM evaluation to compare the results. Higher conversion degrees ($X_{C,gasif} > 0.8$) were omitted in the evaluation because at high conversion degrees ($X_{C,gasif} > 0.8$), the influence of undesired factors such as particle fragmentation on the conversion rate is high. Furthermore, the conversion proceeds slowly at high conversion degrees, resulting in a large amount of data points in the small conversion range from $0.8 \leq X_{C,gasif} \leq 1$, as can be seen from Fig. 14. This would lead to an overvaluing of the conversion behavior at high conversion degrees on the derived kinetics. Fig. 14 illustrates an exemplary data set with adjusted UCM-C model ($0 \leq X_{C,gasif} \leq 0.8$). The parameters f_1 and f_2 were calculated with the derived linear functions (equations (40) and (41). To check the correctness of the UCM-C fitting procedure, the resulting conversion curve (UCM-C, solid black line in Fig. 14) was convoluted with the residence time distribution (the weight function). Fig. 14 reveals that the re-convoluted UCM-C (dashed black line) represents the experimental data (dots) well and therefore confirms the correctness of the procedure.

6.7.1. Influence of imprecisions in the residence time distribution resulting from high steam contents

As mentioned in the foregoing sections, the degree of inaccuracy of system responses increased with increasing steam content. This results in broad errors of f_1 and f_2 as can be seen in Fig. 13. To assess the influence on the derived kinetics, the results from application of UCM-C with the highest and lowest values of f_1 and f_2 were compared to those resulting from f_1 and f_2 determined with the linear fit (equations (40) and (41)) and to the results from UCM fitting (without considering system response behavior). For this comparison, an experimental dataset from a gasification experiment at $T_{Reactor} = 810\ °C$, $p_{tot} = 5\ bar$, $p_{H_2O} = 2\ bar$ (thus $y_{H_2O} = 0.4$) was utilized as a large deviation between the response curves and between the minimum and maximum f_1 and f_2 was observed in step response experiments with this steam content. It was observed for all series of step response experiments evaluated, that the respective maximum value of factor f_1 and the respective maximum value of factor f_2 were always found for the same step response experiment. So both factors either varied with a positive sign or a negative sign, but never in opposite directions.

Fig. 15 shows that the influence of the error in f_1 and f_2 on the resulting reaction rate is small (below 1 %). Parameters f_1 and f_2 are therefore determined with the linear fit (equations (40) and (41)) for the UCM-C.

As gasification experiments were performed with higher steam

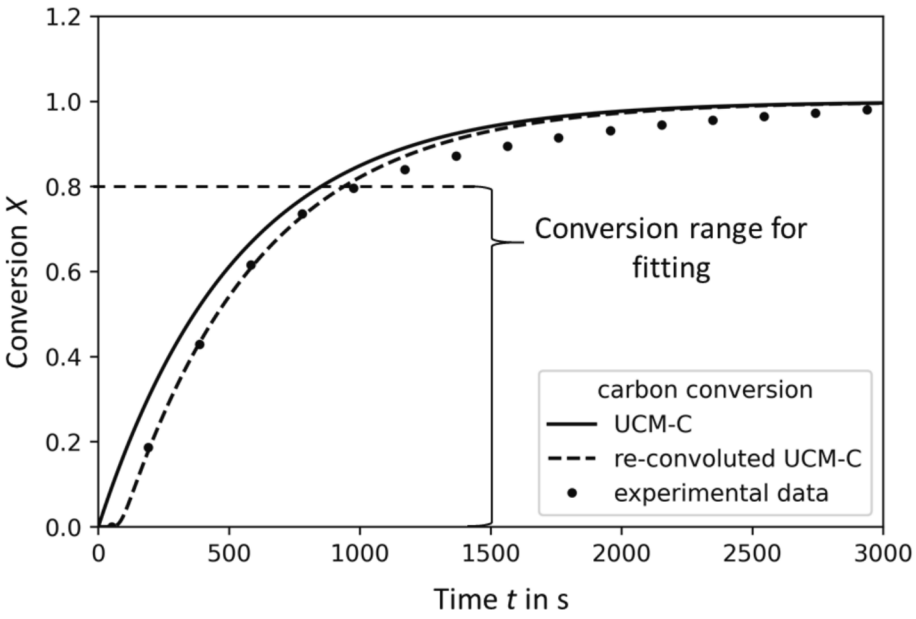

Fig. 14. Gasification experiment at $T_{Reactor} = 850\ °C$, $p_{tot} = 10\ bar$, $p_{H_2O} = 5\ bar$, UCM and UCM-C ($0 \leq X_{C,gasif} \leq 0.8$); verification of the UCM-C procedure by re-convoluting the result.

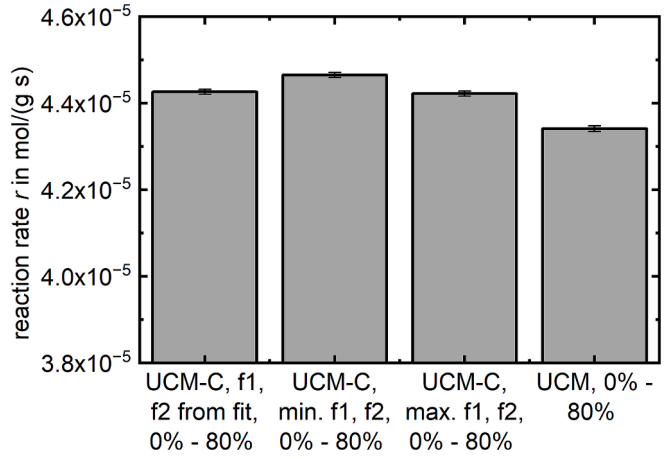

Fig. 15. Comparison of the reaction rate r calculated with UCM-C with minimum, maximum and linearly fitted parameters f_1 and f_2 to the reaction rate calculated directly with UCM. Experimental settings were: $T_{Reactor} = 810\ °C$, $p_{tot} = 5\ bar$, $p_{H_2O} = 2\ bar$.

contents than the step response experiments (up to $y_{H_2O} = 0.625$), parameters f_1 and f_2 were extrapolated following equations (40) and (41) to derive functions of $E(t)$ for these steam contents. Due to the extrapolation, the error in f_1 and f_2 is unknown. To estimate the error resulting from the inaccuracy of the system response for these experiments as well, a sensitivity analysis was done for parameters f_1 and f_2 extrapolated to $y_{H_2O} = 0.625$. f_1 and f_2 were varied between + 30 % and −30 % in steps of 10 %. As already explained before, only variations with either increasing values of f_1 and f_2 (both + 10 %, +20, +30 %) or decreasing values (both −10 %, −20 %, −30 %) are realistic. Resulting reaction rates for the experiments at $T_{Reactor} = 870\ °C$ and $p_{H_2O} = 12.5$ bar are shown for the respective variation of f_1 and f_2 in Fig. 16. The reaction rate for f_1 and f_2 derived from linear fit (equations (40) and (41)) is indicated with a red symbol and a red dashed line. Error bars show the standard deviation of the three repeat experiments.

By means of the results of the sensitivity analysis in Fig. 16, it can be stated that the influence of varying f_1 and f_2 is small (below 0.5 %) and negligible compared to the experimental error from the repeat experiments.

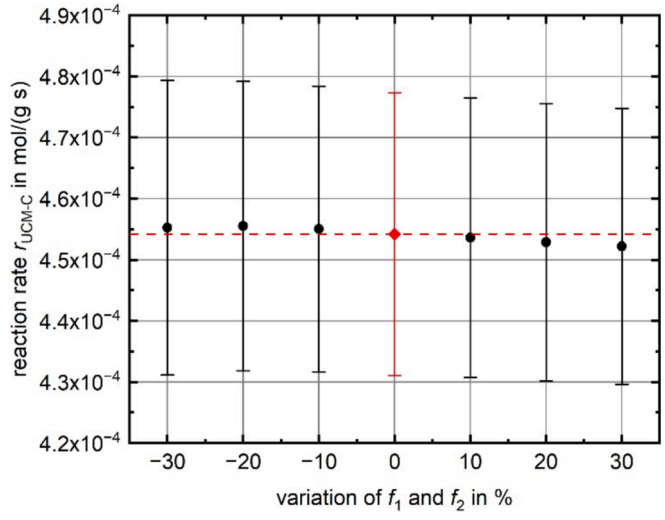

Fig. 16. Sensitivity analysis of the reaction rate r_{UCM-C} with varying parameters f_1 and f_2

6.7.2. Relevance of the system response behavior

The step response experiments from section 6.5. (Fig. 9) showed a strong influence for high steam contents, leading to a wide residence time distribution. In addition, the experiments with the highest steam partial pressures (accordingly steam contents) are those with the highest reaction rates. The reactions rates from UCM-C evaluation as well as from UCM evaluation for $0 \leq X_{C,gasif} \leq 0.8$ were compared for the experimental data set as described in section 3.1., Table 1. Fig. 17 summarizes the resulting reaction rates as well as the reaction rates published by Schneider et al. [19] for the same char quality.

A continuous transition between the reaction rates at low partial pressures by Schneider et al. and the reaction rates at higher partial pressures determined by UCM-C evaluation in this work for each reaction temperature can be recognized. Thus, the data from Schneider et al. and the data from UCM-C evaluation from this work match up very well. As expected, he reaction rates increase with increasing H_2O partial pressure and increasing temperature.

For the lower reaction rates at 810 °C and 830 °C up to 10 bar steam partial pressure determined in this work, the rates derived from UCM respectively UCM-C evaluation are similar (encircled with grey lines). With increasing steam partial pressure and increasing reaction temperature, an increasing difference between the rates resulting from the two evaluation procedures becomes obvious.

In Fig. 17, especially the experiments at $T_{Reactor} = 870$ °C and $p_{H_2O} = 12.5$ bar are standing out because of the large deviation and the decrease of the reaction rate by UCM at $p_{H_2O} = 12.5$ bar. The experimentally derived carbon conversion, the corresponding UCM and UCM-C models (both adjusted to $0 \leq X_{C,gasif} \leq 0.8$) and the residence time distribution for an experiment at $T_{Reactor} = 870$ °C and $p_{H_2O} = 12.5$ bar ($y_{H_2O} = 0.625$) are shown in Fig. 18. The residence time distribution for the steam content of $y_{H_2O} = 0.625$ was calculated as in section 6.6. with (40) and (41). Qualitatively, the spread of the residence time distribution is large compared to the time-course of the conversion $X_{C,gasif}(t)$. A comparison of the UCM adjustment (orange line) and adjustment of UCM-C (green and red dotted line) shows poor fit quality of the UCM adjustment. The shape of the time-course of the experimentally derived conversion cannot be described by the UCM, while re-convolution of the UCM-C derived conversion curve with the residence time distribution reveals a better fit accuracy.

To understand the influence of the spread of the residence time distribution, values for $1/R_{UCM-C}$ determined by application of UCM-C (averaged for the repeat experiments) and spreads of the residence time distributions $E(t)$ (calculated as in section 6.6. with (40) and (41)) are compiled in Table 5 For experiments at $T_{Reactor} = 870\ °C$ and $p_{H_2O} = 12.5$ bar ($y_{H_2O} = 0.625$; as shown in Fig. 18), the spread of the residence time distribution is approximately 174 s and $1/R_{UCM-C} = 183$ s. The ratio $(1/R_{UCM-C})/E(t)$ is approximately 1. This suggests that the relevance of the system response behavior can be estimated by comparing $1/R_{UCM-C}$ and the width of $E(t)$ in a comparable manner as proposed by Stoesser et al. by means of the system response time [2].

In Table 6 and in Fig. 17, experiments are underlined respectively encircled in grey, when the reaction rates derived by UCM and UCM-C are similar. It results that for ratios $(1/R_{UCM-C})/E(t) \geq 6$, the influence of the system response behavior on the derived reaction kinetics can be neglected. For ratios inferior to that, the system response behavior has to be included in the evaluation method.

7. Summary and conclusion

A differential fixed bed reactor (dFBR) for reaction kinetic measurements developed at KIT was described. Gasification experiments with biogenic char and H_2O were conducted at steam partial pressures up to 12.5 bar, total pressures up to 20 bar and temperatures up to 870 °C. During the experiments, the product gas composition was analyzed. The carbon conversion was determined by C-, O- and H-

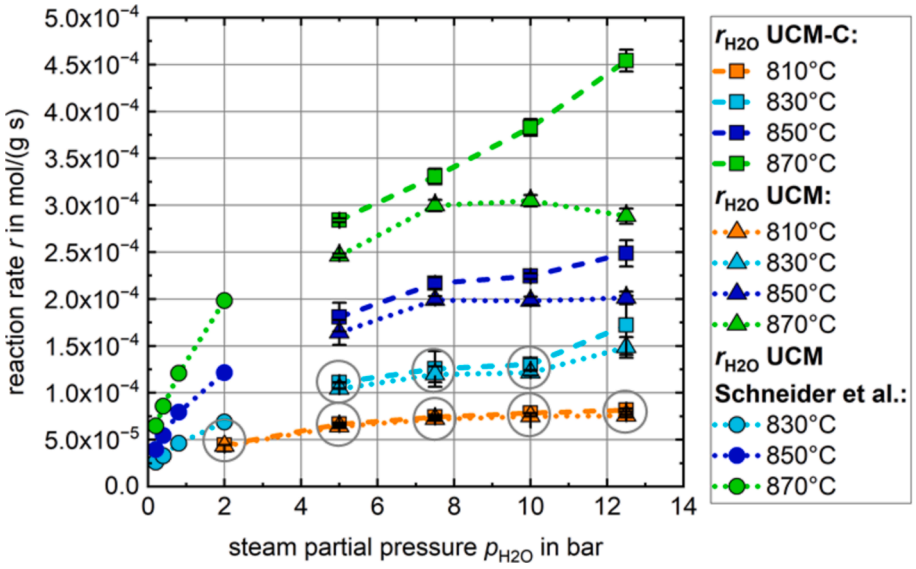

Fig. 17. Reaction rates at different steam partial pressures between 2 bar and 12.5 bar and reaction rates determined by Schneider et al. [19] for the same secondary char qualities.

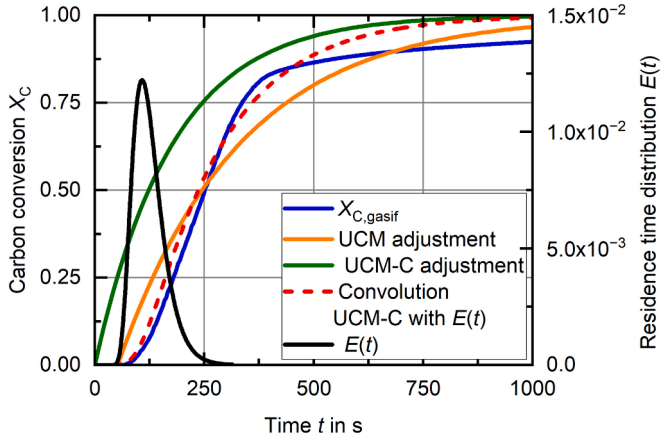

Fig. 18. Experimental carbon conversion, UCM and UCM-C fits, corresponding residence time distribution E(t) and re-convolution of UCM-C with E(t) for a gasification experiment at $p_{H_2O} = 12.5\ bar$ and $T_{Reactor} = 870\ °C$ ($y_{H_2O} = 0.625$).

Table 6
Averaged values for $1/R_{UCM-C}$ determined by application of UCM-C and spreads of the residence time distributions $E(t)$.

$T_{Reactor}$	p_{tot}	p_{H_2O}	$1/R_{UCM-C}$	Spread of E(t)	Ratio $(1/R_{UCM-C})/E(t)$
°C	bar	bar	s	s	–
810	5	2	1881	87	22
	10	5	1249	112	11
	20	7.5	1120	82	14
	20	10	1063	112	9
	20	12.5	1022	174	6
830	10	5	750	112	7
	20	7.5	667	82	8
	20	10	639	112	6
	20	12.5	487	174	3
850	10	5	464	112	4
	20	7.5	384	82	5
	20	10	371	112	3
	20	12.5	336	174	2
870	10	5	293	112	3
	20	7.5	252	82	3
	20	10	217	112	2
	20	12.5	183	174	1

balancing.

The evaluation of the experimental data relies on the assumption of a differential fixed bed, meaning that the conversion of the gas phase and the resulting changes in gas composition do not influence the reaction kinetics in axial direction of the sample bed. To verify the differential operation, a new criterion derived from the first Damköhler number was developed. With this criterion for a differential system, the threshold value of the reaction gas concentration $c_{i,H}$ leaving the differential fixed bed related to the concentration entering $c_{i,0}$ was $c_{i,H}/c_{i,0} \geq 0.9$. It resulted that with the applied sample masses of 10 mg to 50 mg, the threshold value was not exceeded and reproducible experimental results were obtained with all applied sample masses.

During the gasification experiments, the product gas composition determined by the gas analyzers was not only influenced by the reaction kinetics but also by the system response behavior. This led to biased apparent conversion rates. To solve this problem, the system response behavior was investigated for a reasonable range of reactor temperatures, total pressures and gas compositions. A mathematical description of the system response behavior based on the axial dispersion model was derived and then integrated into the evaluation routine of the reaction kinetic data. The reciprocal value of the reactivity $1/R_{UCM-C}$ was compared to the spread of the residence time distribution E(t). Increasing steam partial pressures and reaction temperatures lead to decreasing values of $1/R_{UCM-C}$. Meanwhile, high steam partial pressures lead to broader residence time distributions due to the system-specific behavior. It was found that for ratios of $1/R_{UCM-C}$ divided by the spread of E(t) of six or lower, the system response behavior relevantly affected the experimental results. To account for the influence of the water content on the residence time distribution, an empirical, application-oriented approach describing the dependence of the system response on the steam content was included into the mathematical description of the system response behavior.

CRediT authorship contribution statement

Stella Walker: Writing – review & editing, Writing – original draft, Visualization, Validation, Software, Methodology, Investigation, Formal analysis, Conceptualization. **Thomas Kolb:** Writing – review & editing, Supervision, Project administration, Funding acquisition.

Declaration of competing interest

The authors declare that they have no known competing financial interests or personal relationships that could have appeared to influence the work reported in this paper.

Acknowledgements

The authors gratefully acknowledge the financial support by the Helmholtz Association of German Research Centers (HGF), within the research program Energy Efficiency, Materials and Resources (EMR). Further acknowledgement goes to Prof. Dr.-Ing. Thomas Meurer (KIT, Institute of Mechanical Process Engineering and Mechanics, Digital Process Engineering) and Pascal Jerono (KIT, Institute of Mechanical Process Engineering and Mechanics, Digital Process Engineering) for fruitful discussions and to Prof. Dr.-Ing. Sonia Lucía Rincón Prat (Universidad Nacional de Colombia, Engineering Faculty, Research Group on Biomass and Optimization of Thermal Systems BIOT), Paul Moog (KIT) and Lukas Springmann (formerly KIT) for their experimental support and Helmut Reis (KIT, Institute for Technical Chemistry) for the photographies.

Appendix A. Supplementary data

Supplementary data to this article can be found online at https://doi.org/10.1016/j.fuel.2024.133561.

Data availability

Data will be made available on request.

References

[1] Kolb T, Aigner M, Kneer R, Müller M, Weber R, Djordjevic N. Tackling the challenges in modelling entrained-flow gasification of low-grade feedstock. J Energy Inst 2016;89:485–503. https://doi.org/10.1016/j.joei.2015.07.007.
[2] Stoesser P, Schneider C, Kreitzberg T, Kneer R, Kolb T. On the influence of different experimental systems on measured heterogeneous gasification kinetics. Appl Energy 2018;211:582–9. https://doi.org/10.1016/j.apenergy.2017.11.037.
[3] Rossberg M, Wicke E. Transportvorgänge und Oberflächenreaktionen bei der Verbrennung graphitischen Kohlenstoffs. Chem Ing Tech 1956;28:181–9. https://doi.org/10.1002/cite.330280309.
[4] Kibria MA, Sripada P, Bhattacharya S. Rational design of thermogravimetric experiments to determine intrinsic char gasification kinetics. Proc Combust Inst 2019;37:3023–31. https://doi.org/10.1016/j.proci.2018.07.085.
[5] Baath YS, Nikrityuk PA, Gupta R. Experimental and numerical verifications of biochar gasification kinetics using TGA. Renew Energy 2022;185:717–33. https://doi.org/10.1016/j.renene.2021.12.091.
[6] Dammann M, Walker SC, Mancini M, Kolb T. Devolatilisation of beech wood char: Kinetics from thermogravimetric analyses and drop-tube reactor experiments. Fuel 2024;375:131967. https://doi.org/10.1016/j.fuel.2024.131967.
[7] Gövert B, Pielsticker S, Kreitzberg T, Habermehl M, Hatzfeld O, Kneer R. Measurement of reaction rates for pulverized fuel combustion in air and oxyfuel atmosphere using a novel fluidized bed reactor setup. Fuel 2017;201:81–92. https://doi.org/10.1016/j.fuel.2017.03.009.
[8] Haustein HD, Kreitzberg T, Gövert B, Massmeyer A, Kneer R. Establishment of kinetic parameters of particle reaction from a well-stirred fluidized bed reactor. Fuel 2015;158:263–9. https://doi.org/10.1016/j.fuel.2015.05.038.
[9] Komarova E, Guhl S, Meyer B. Brown coal char CO2-gasification kinetics with respect to the char structure. Part I: Char structure development, Fuel 2015;152:38–47. https://doi.org/10.1016/j.fuel.2015.01.107.
[10] Netter T, Geißler A, Spliethoff H. Determination of the intrinsic gasification kinetics of a bituminous coal including product gas inhibition and char deactivation under entrained flow conditions. J Energy Res Technol 2020;142:070913. https://doi.org/10.1115/1.4046142.
[11] Gonzalez V, Rußig S, Schurz M, Krzack S, Kleeberg J, Guhl S, et al. Experimental investigations on lignite char gasification kinetics using a pressurized drop tube reactor. Fuel 2018;224:348–56. https://doi.org/10.1016/j.fuel.2018.03.018.
[12] Baerns M, Behr A, Brehm A, Gmehling J, Hinrichsen K-O, Hofmann H, et al. Technische chemie. 2nd ed. Wiley-VCH; 2013.
[13] Jordan DG. Chemical process development. Interscience Publishers; 1968.
[14] Dusan Boskovic, Experimentelle Bestimmung und Modellierung des Verweilzeitverhaltens mikrofluidischer Strukturen, 2010.
[15] Ekambara K, Joshi JB. Axial mixing in laminar pipe flows. Chem Eng Sci 2004;59:3929–44. https://doi.org/10.1016/j.ces.2004.05.025.
[16] Abad A, Cardona SC, Torregrosa JI, López F, Navarro-Laboulais J. Flow analysis deconvolution for kinetic information reconstruction. J Math Chem 2005;38:271–92. https://doi.org/10.1007/s10910-005-5422-8.
[17] Sarraguça JMG, Lopes JA, Santos JLM, Lima JLFC. Mathematical simulation of signal profiles in flow analysis. Anal Lett 2012;45:85–98. https://doi.org/10.1080/00032719.2011.582551.
[18] Schneider C, Walker S, Phounglamcheik A, Umeki K, Kolb T. Effect of calcium dispersion and graphitization during high-temperature pyrolysis of beech wood char on the gasification rate with CO2. Fuel 2021;283:118826. https://doi.org/10.1016/j.fuel.2020.118826.
[19] Schneider C, Zeller M, Böhm D, Kolb T. Influence of pressure on the gasification kinetics of two high-temperature beech wood chars with CO2, H2O and its mixture. Fuel 2021;299:120523. https://doi.org/10.1016/j.fuel.2021.120523.
[20] Wang Y, Bell DA. Competition between H 2 O and CO 2 during the gasification of Powder River Basin coal. Fuel 2017;187:94–102. https://doi.org/10.1016/j.fuel.2016.08.109.
[21] Fermoso J, Stevanov C, Moghtaderi B, Arias B, Pevida C, Plaza MG, et al. High-pressure gasification reactivity of biomass chars produced at different temperatures. J Anal Appl Pyrol 2009;85:287–93. https://doi.org/10.1016/j.jaap.2008.09.017.
[22] Wang G, Zhang J, Shao J, Liu Z, Wang H, Li X, et al. Experimental and modeling studies on CO2 gasification of biomass chars. Energy 2016;114:143–54. https://doi.org/10.1016/j.energy.2016.08.002.
[23] Zhao S, Ding L, Ruan Y, Bai B, Qiu Z, Li Z. Experimental and kinetic studies on steam gasification of a biomass char. Energies 2021;14:7229. https://doi.org/10.3390/en14217229.
[24] Emig G, Klemm E. Chemische reaktionstechnik. 6th ed.,. Springer-Verlag GmbH; 2017.
[25] Levenspiel O. Chemical reaction engineering. 3rd ed. John Wiley & Sons; 1999.
[26] D. Christ, The effect of char kinetics on the combustion of pulverized coal under oxyfuel conditions, 1. Aufl., Sierke, Göttingen, 2013.
[27] Mueller A, Haustein HD, Stoesser P, Kreitzberg T, Kneer R, Kolb T. Gasification kinetics of biomass- and fossil-based fuels: comparison study using fluidized bed and thermogravimetric analysis. Energy Fuels 2015;29:6717–23. https://doi.org/10.1021/acs.energyfuels.5b01123.
[28] H. Eilers, Flexibler Betrieb der Fischer-Tropsch-Synthese - Katalysator- und Reaktorverhalten mit Co in der 3-Phasen-Blasensäule, (n.d.).
[29] Aris R. On the dispersion of a solute in a fluid flowing through a tube. Proc Roy Soc London Ser A 1956.
[30] Ananthakrishnan V, Gill WN, Barduhn AJ. Laminar dispersion in capillaries: Part I. Mathematical analysis, AIChE J 1965;11:1063–72. https://doi.org/10.1002/aic.690110620.
[31] Reejhsinghani NS, Gill WN, Barduhn AJ. Laminar dispersion in capillaries: Part III Experiments in horizontal tubes including observations on natural convection effects. AIChE J 1966;12:916–21. https://doi.org/10.1002/aic.690120515.
[32] Stephan P, Kabelac S, Kind M, Mewes D, Schaber K, Wetzel T. VDI-Wärmeatlas. 12th ed.,. Springer-Verlag GmbH; 2019.
[33] Gövert B. Char combustion kinetics using a micro fluidized bed reactor. Rheinisch-Westfälische Technische Hochschule Aachen 2018.